JOURNAL OF GEOMETRIC MECHANICS
©American Institute of Mathematical Sciences
Volume **12**, Number **3**, September **2020**

doi:10.3934/jgm.2020021

pp. **455–505**

ANGULAR MOMENTUM COUPLING, DIRAC OSCILLATORS, AND QUANTUM BAND REARRANGEMENTS IN THE PRESENCE OF MOMENTUM REVERSAL SYMMETRIES

Toshihiro Iwai

Department of Applied Mathematics and Physics
Kyoto University
Kyoto 606, Japan

Dmitriĭ A. Sadovskiĭ and Boris I. Zhilinskiĭ*

Department of Physics
Université du Littoral—Côte d'Opale
59140 Dunkerque, France

Dedicated to James Montaldi

Abstract. We investigate the elementary rearrangements of energy bands in slow-fast one-parameter families of systems whose fast subsystem possesses a half-integer spin. Beginning with a simple case without any time-reversal symmetries, we analyze and compare increasingly sophisticated model Hamiltonians with these symmetries. The models are inspired by the time-reversal modification of the Berry phase setup which uses a family of quadratic spin-quadrupole Hamiltonians of Mead [Phys. Rev. Lett. **59**, 161–164 (1987)] and Avron *et al* [Commun. Math. Phys. **124**(4), 595–627 (1989)]. An explicit correspondence between the typical quantum energy level patterns in the energy band rearrangements of the finite particle systems with compact slow phase space and those of the Dirac oscillator is found in the limit of linearization near the conical degeneracy point of the semi-quantum eigenvalues.

1. **Introduction.** The interest in the geometric and topological properties of parametric families of quantum Hamiltonians was largely stimulated by the seminal paper of Michael Berry [10], who analyzed the evolution of the spin states with spin $S = \frac{1}{2} \approx \|\boldsymbol{S}\|$ in the presence of the magnetic field $\boldsymbol{B}$. The system is governed by the linear Hamiltonian

$$\hat{H} = \boldsymbol{B} \cdot \hat{\boldsymbol{S}}. \tag{1}$$

When $\boldsymbol{B}$ is made to vary adiabatically slowly, following a closed path in the regular domain $\mathbb{R}^3_{\boldsymbol{B}} \setminus \{0\}$ of the parameter space, the eigenstates of (1) acquire a *geometric phase* [10, 43]. This phase can be seen as both a consequence and an indicator of the nontrivial topology of the system. To examine the topology more fully, we study the two eigenstate bundles defined by the eigenvalues $\lambda_{1,2}(\boldsymbol{B})$ with $S = \frac{1}{2}$. Away from the degeneracy at $\boldsymbol{B} = 0$, and more specifically, over any sphere $\mathbb{S}^2$

2020 *Mathematics Subject Classification.* Primary: 37J05, 81Q70, 81V55; Secondary: 53C80, 58J70, 70G45.

Key words and phrases. Energy bands, Chern number, time reversal, geometric phase, semi-quantum approach, quantum-classical correspondence, Dirac oscillator.

* Corresponding author: Boris I. Zhilinskiĭ.

surrounding the origin in $\mathbb{R}^3_{\boldsymbol{B}}$, and in particular over $\{\boldsymbol{B}, \|\boldsymbol{B}\| = 1\}$, we find that $\lambda(\boldsymbol{B})$ define regular complex line bundles with Chern index $c_1 = 1$ or -1.

1.1. **Formal and dynamical control parameters. Their number.** We like to point out that the parameters $\boldsymbol{B}$ in (1) can be chosen and changed at will within their domain and without any feedback from the system with Hamiltonian (1). In other words, $\boldsymbol{B}$ are not influenced in any way by the dynamics of the system. We will call such control parameters *formal*, *plain*, or *tuning*. Their physical origins should not obscure their formal character[1]. At the same time, parameters whose evolution is governed by the Hamiltonian of the system itself, i.e., whose (adiabatically slow) variation provokes a feedback from the fast system, will be called *dynamical*. In our work, we focus on slow–fast systems[2] with dynamical parameters. Dynamical parameters play the role of control parameters only in the semi-quantum system (see sec. 1.3). At the same tme, they are dynamical variables of the complete system and of its slow subsystem.

The eigenstates of systems with a finite number of states, such as the system with Hamiltonian (1), are given by the eigenvectors of Hermitian matrices. The codimension of degeneracy of two eigenvalues of a general Hermitian matrix, regardless the dimension of the matrix itself (in other words, for any spin), is *three* [41, 1, 21]. So in the particular case of (1) and for $S = \frac{1}{2}$, the eigenvalues of the 2×2 Hermitian matrix become degenerate in one single point $B = 0$. We conclude that in general, we may be interested in systems with one slow degree of freedom (two dynamical parameters) and one formal control parameter (see examples in sec. 1.3). In the presence of additional symmetries (sec. 2.3, 4, 5), the matrix of the quantum Hamiltonian and its spectrum may have specific additional properties. In particular, the minimal number of semi-quantum states (the dimension of the matrix) required to observe typical spectra, the kind of degeneracy, and the codimension may vary.

1.2. **Semiclassical eigenstate bundles.** It is important to notice that in general, with regard to parameters of the system, we distinguish two kinds of semi-quantum eigenstate bundles which we will denote Λ and Δ. The base space of Λ is always the slow classical phase space P whose coordinates are dynamical parameters. This P is not necessarily a sphere, and it may not even be compact. The Λ bundle can be

[1] A particularly instructive example with *formal* control parameters q of dynamical origin is the phase of the electronic wavefunctions Ψ_{el} in the Jahn–Teller systems. Herzberg and Longuet-Higgins [19] considered such systems within the Born-Oppeheimer approximation, where nuclear coordinates q play the role of control parameters of the separated electronic Hamiltonian H_{el}. Their work anticipated the geometrical phase analysis by Berry [10] and is widely known in molecular physics [32]. The nontrivial topological contribution to the phase of Ψ_{el} is associated with the close loop around the degeneracy point of two electronic potential energy surfaces in the q-space. While being plain control parameters of H_{el}, the nuclear coordinates q are dynamical variables for the complete electronic-nuclear Hamiltonian or, equally, for the separated Hamiltonian H_{nucl} describing the slow vibrations of the nuclei. We like to stress that q are formal and *not* dynamical control parameters of the fast electronic subsystem because H_{el} has no influence on their evolution. In other words, q get no feedback from the fast system. On the other hand, the reason why dynamical parameters remain influenced explicitly by the fast system in the semi-quantum description of our systems (sec. 2, 3, 4, and 5) is in the nature of their slow-fast separation which applies only on the complement to the open saturated neighbourhood of the degeneracy point (bounded by the base space of Δ, see sec. 1.3) in the formal-dynamical control parameter space.

[2] Dynamical variables of slow-fast systems fall in two cathegories with strongly different rates of variation and respective time scales. Under certain conditions, this allows separation into slow and fast subsystems. There is a wast literature on slow-fast dynamical systems which are ubiquitous in applications, see, for example, [8, 34, 35].

called *global*. The base space of Δ is a sphere surrounding the degeneracy point in the total (dynamical-formal) control parameter space. The Δ bundle is considered in the geometric phase framework. We may call it *local*. In the example in sec. 2.1, Λ and Δ are the same bundle, while in sec. 2.2 they are rather different. In sec. 3 and 4, both Λ and Δ are bundles over a sphere, but one is parameterized by dynamical parameters, while the other—by formal and dynamical control parameters. In the space of all parameters, the base spaces of Λ and Δ intersect (appendix A.4). They have common closed loops parameterized entirely by dynamical variables for fixed formal control parameters. Furthermore, such loops may be periodic orbits of the slow classical system. Such periodic orbits exhibit *dynamical geometric phase* given by the Chern index of Δ. Semiclassical quantization [17, Appendix A] provides one possible manifestation of such phase.

We observe further that global bundles Λ form continuous parametric families with regard to regular values of tuning control parameter(s) μ, while there is one single local Δ bundle for each degeneracy point (tuning parameters are often choosen so that degeneracies occur for critical value $\mu = 0$). When tuning parameters μ have several disconnected open domains of regular values (such as, in the simplest case, two intervals with $\mu < 0$ and $\mu > 0$), the c_1 indices of Λ bundles on each domain may differ and the difference(s) δc_1 or *delta-Chern* characterize the degeneracy point(s). At the same time, the c_1 indices of Δ bundles contribute to δc_1 (appendix A.4). While the Δ bundle construction ignores any differences between the dynamical and formal control parameters, Λ bundles have an important dynamical interpretation. Their index characterizes the number of slow quantum states which can be supported on P and this relates δc_1 to the number of redistributed quantum states, see more in sec. 1.3.

1.3. **Quantum, semi-quantum, and classical.** Dynamical parameterization enhances considerably the object of our study and places it at crossroads of several powerful mathematical theories. It becomes universally important to many physical applications.

Within the geometric phase setup, we obtain a "fast" quantum system on a finite Hilbert space $\mathcal{H}_{\text{fast}}$ of low dimension (e.g., two for $S = \frac{1}{2}$). The Hamiltonian of this system is a combination of operators acting on $\mathcal{H}_{\text{fast}}$ with coefficients depending on classical dynamical variables (q, p) of the "slow" system and, possibly, additional formal control parameters μ which are also meant to be varied adiabatically slowly (see footnote 2). The eigenstates are obtained as eigenvectors of a low-dimensional Hermitian matrix whose eigenvalues $\lambda(q, p)$ play the role of classical Hamiltonians governing the dynamics of the slow system corresponding to each fast eigenstate. We call this description *semi-quantum*.

At the same time, the fast and slow systems can be both treated as quantum and can be described using the Hilbert space $\mathcal{H}_{\text{fast}} \times \mathcal{H}_{\text{slow}}$. Since the slow system has a close and well defined classical limit, $\mathcal{H}_{\text{slow}}$ is typically a much larger space, and, if the underlying slow classical phase space is non-compact, $\mathcal{H}_{\text{slow}}$ is infinite (Dirac equation, Dirac oscillator in sec. 2.2). Different time-scales (footnote 2) result in a specific structure of the energy spectrum and the localization patterns of the quantum states of such system. The spectrum consists of *bands* with relatively large density and number of states. Transitions between the states within a band correspond to excitations in the slow degree of freedom, and, in most basic situations, energy alone is enough to separate the bands: the in-band splittings are considerably smaller than the gaps between the bands. In regular cases, the number

of energy bands equals the number of semi-quantum eigenvalues. When the latter have a degeneracy, the bands merge and exchange energy levels. The reason for this exchange is in the nature of the dynamical parameterization of the fast system. Near the degeneracy point, due to the interaction between the two subsystems, the separation of the slow and fast dynamics becomes blurred, and certain states localized near the degeneracy may change their character and switch bands. We conclude that the degeneracy of semi-quantum eigenvalues is the cause of both the geometric phase and this *redistribution phenomenon*.

To realize how considerable the relation and the interplay between the geometric phase and the energy level redistribution is, we like to go a bit further into the structure of the bands. For nondegenerate (typical) singularities, the number of the exchanged states is much smaller than that of the states in the bands. In fact, most of the levels are never exchanged and continue always within the same band. We call them "bulk" states. Their number is given roughly by the symplectic volume of the underlying compact slow classical phase space and may be obtained using an appropriate quantization scheme (sec. 2.1). In the non-compact setting, this can be generalized using fractional formal Chern number (70) in Appendix A.3. The few levels that can and do get exchanged are the "edge" states. In this context, the *correlation diagrams* showing how levels continue when parameters cross the degeneracy point become very instrumental and are employed throughout the article (sec. 3, 4, and 5). The Chern index characterizing the bundle Λ of semi-quantum eigenvalues over the slow phase space gives, essentially, the number of missing/excessive edge states [11, 12, 13, 21, 22, 23, 25]. More specifically, this index gives the quantity by which the actual number of states in the band differs from that given by the symplectic volume of the underlying classical phase space. The same index, but computed for bundle Δ gives the geometric phase, and it can be conjectured that computation for all local Δ bundles gives the number of redistributed states. For further generalization of the analysis of the redistribution phenomenon, an application of the Atiyah-Singer index theorem [2, 3, 4] and geometric quantization principles [15] seems to be relevant.

The last but not the least, although being the least exploited in our present work, comes the fully classical description. Singularities of the slow-fast classical mechanical system with several (at least two) degrees of freedom are related to the semi-quantum degeneracies and, therefore, to the edge state redistribution. In particular, if the slow-fast system is integrable, such singularities are at the origin of *Hamiltonian monodromy* [37].

1.4. **Main purpose and outline.** Dynamical modifications of the original setup (1) open a large domain of diverse and versatile mathematical theory and applications which go far beyond the original geometric phase analysis. The latter remains, however, a vital organizing tool in the study of different dynamical parametric systems. Our main interest in this work is in the phenomenon of redistribution between the energy bands in the slow-fast systems [12], and so we focus primarily on the full quantum system and its relation to the semi-quantum description. Among different symmetry properties which can be appropriate for concrete physical systems there is one particular property, the time reversal invariance (see note 5), which is considered as rather general due to its relevance across a very wide class of physical systems. In this work, we focus on time-reversal-invariant dynamical modifications. We also prefer uncovering systems which are fundamental and important to atomic and molecular (finite particle) applications. As a consequence, we analyze

semi-quantum systems with compact slow phase spaces (such as the simple angular momentum coupling system in sec. 2.1) and relate them to non-compact examples (such as the Dirac oscillator in sec. 2.2) through linearization (sec. 2.1.4) and local description near the degeneracy of their semi-quantum eigenvalues. The linearized systems with non-compact slow phase spaces may in turn be of importance to other fields, notably in solid state physics. The eventual distant but much desired outcome of this approach is a universal theory of redistribution phenomena.

In the context of sec. 1.3, the interest in finding dynamical equivalents of time-reversal invariant modifications by Mead [31] and Avron *et al* [5] of the original geometric phase setup (1) is quite substantial. As we explain in sec. 2.3, the system with the quadratic spin-quadrupole Hamiltonian [31, 5] has co-dimension 5, and, therefore, its dynamical analogues can have a slow phase space P of maximal dimension 4, i.e., four dynamical and one formal control parameter. In our present work, however, we remain at the level of systems with only two dynamical parameters (one slow degree of freedom). Furthering substantial understanding of such systems allows uncovering possible consequences of the additional symmetries imposed in [31, 5] and is a necessary precursor investigation in preparation for larger dynamical models (sec. 6).

We outline the plan of the article. In sec. 2 we discuss two basic dynamical modifications of (1) along with its time-reversal modification [5, 6]. In sec. 3 we return to the historically first simple dynamical modification of (1) suggested very early in 1988 [36] and analyzed further in [37, 11, 21]. Here we uncover the exact relation of this system to the Dirac oscillator.

The progression of different systems analyzed further in the paper is chosen so that the description of preceding simpler systems in sec. 2 and 3 helps towards understanding subsequent systems, with increasingly smaller effort, through linearization, deformation, and discrete symmetry reduction. So turning to time-reversal-invariant systems in sec. 4, we come up with an angular momentum system whose Hamiltonian can be regarded as the most basic time-reversal deformation of the spin-orbit coupling term in sec. 2.1, itself the most natural and basic dynamical modification of the original Hamiltonian (1). It turns out that there is a 1:2 correspondence between this system and the non-symmetric case in sec. 3 and its Dirac oscillator linearization. As a consequence, Chern indices c_1 and their change δc_1 can be deduced essentially from the results in sec. 3. Otherwise, Chern indices can be computed directly for our model systems as detailed in Appendix A.

Finally, in sec. 5, we consider dynamical modifications of quadratic spin systems in [31, 5, 6] with spin $\frac{3}{2}$. We continue using angular momentum slow systems. Our particular modification has the time-reversal invariance group of order four including both the $\mathcal{T}_S$-symmetry of quadratic spin systems (sec. 2.3) and the $\mathcal{T}$-symmetry of systems with two angular momenta (sec. 2.1 and 4). Furthermore, like in all our spin-$\frac{1}{2}$ systems (sec. 2.1, 3, and 4), we have only one slow degree of freedom, which is, in this case, not the maximal possibility. With the minimal number of dynamical parameters, the redistribution phenomena in such quadratic spin-orbit systems turn out to be in 1:2 correspondence with the preceding spin-$\frac{1}{2}$ $\mathcal{T}$-invariant system in sec. 4. However, while four individual levels get exchanged between the bands, the total number of states in the bands remains unchanged, i.e., redistributions occur "both ways" and the bulk phenomenon amounts to 0. The detailed Chern index analysis reflects the topological origins of this arrangement.

2. **Three basic examples.** We begin with simple modifications of the original setup with Hamiltonian (1) which illustrate sec. 1.1 and 1.3. The details in each example are instructive to follow. They help understanding the key elements in the analysis of the systems in sec. 3, 4, and 5.

2.1. **Spin-orbit coupling.** One of the simplest and most direct dynamical analogues of (1) is the Hamiltonian

$$\hat{H} = \boldsymbol{N} \cdot \hat{\boldsymbol{S}}, \tag{2a}$$

where $\boldsymbol{N}$ represents the mechanical angular momentum of the system. In atomic physics, this momentum is called orbital and denoted by $\boldsymbol{L}$, but for us its physical origin can lie elsewhere, e.g., it can be associated with a degenerate molecular vibration, or with the overall rotation of a molecule. Nevertheless, for brevity, we like to call the right hand side of (2a) the *spin-orbit coupling* term.

As discussed in sec. 1.3, dynamically parameterized semi-quantum Hamiltonian (2a), is accompanied by the fully quantum Hamiltonian

$$\hat{H} = \hat{\boldsymbol{N}} \cdot \hat{\boldsymbol{S}}, \tag{2b}$$

and the fully classical Hamiltonian

$$H = \boldsymbol{N} \cdot \boldsymbol{S}. \tag{2c}$$

Since both $\|\boldsymbol{N}\|$ and $\|\boldsymbol{S}\|$ Poisson commute with (2c), we can fix respective values[3] of N and S when analyzing systems with Hamiltonians (2). This means that the classical (slow) phase space of the semi-quantum system is the 2-sphere $\mathbb{S}^2_N$, the set of all orientations[4] of $\boldsymbol{N}$. Furthermore, the phase space of the fully classical system is $\mathbb{S}^2\times\mathbb{S}^2$, while the $(2S+1)(2N+1)$-dimensional Hilbert space of the corresponding fully quantum system

$$\mathcal{H}_{S,N} = \mathcal{H}_S \otimes \mathcal{H}_N$$

is spanned by eigenfunctions $|S,\sigma\rangle|N,\eta\rangle$ of $\hat{S}_1$ and $\hat{N}_1$, such that

$$\hat{S}_1|S,\sigma\rangle|N,\eta\rangle = \sigma\,|S,\sigma\rangle|N,\eta\rangle \quad \text{and} \quad \hat{N}_1|S,\sigma\rangle|N,\eta\rangle = \eta\,|S,\sigma\rangle|N,\eta\rangle$$

with $\sigma = -S, -S+1, \ldots, S-1, S$ and $\eta = -N, -N+1, \ldots, N-1, N$. The above basis implies well separated fast and slow subsystems and is called *uncoupled*.

2.1.1. *The semi-quantum system with spin* $\frac{1}{2}$. For a given fast system with spin S, the semi-quantum Hamiltonian (2a) becomes a $(2S+1)$-dimensional Hermitian matrix defined on $\mathbb{S}^2_N$. Rewriting (2a) in terms of so(3) ladder operators

$$N_\pm = N_2 \pm \mathrm{i}N_3 \text{ and } \hat{S}_\pm = \hat{S}_2 \pm \mathrm{i}\hat{S}_3, \tag{3}$$

we can find its matrix from the action of $\hat{S}_\pm$ on $|S,\sigma\rangle$. Specifically, using

$$\langle \tfrac{1}{2},\tfrac{1}{2}|\hat{S}_+|\tfrac{1}{2},-\tfrac{1}{2}\rangle = \langle \tfrac{1}{2},-\tfrac{1}{2}|\hat{S}_-|\tfrac{1}{2},\tfrac{1}{2}\rangle = \sqrt{\left(S+\tfrac{1}{2}\right)\left(S-\tfrac{1}{2}+1\right)} = 1\ ,$$

we arrive at the $S=\frac{1}{2}$ spinor representation of (2a)

$$\hat{H} = \frac{1}{2}\begin{pmatrix} -N_1 & N_+ \\ N_- & N_1 \end{pmatrix} \tag{4}$$

[3] In this work, unless indicated explicitly, we shall assume $N \gg 1$ and imply $\|\boldsymbol{N}\| = \hbar\, N$ instead of the quantum relation $\|\boldsymbol{N}\| = \hbar\sqrt{N(N+1)}$, or the semiclassical formula $\|\boldsymbol{N}\| = \hbar(N+\frac{1}{2})$. Furthermore, atomic units with $\hbar = 1$ will be used throughout the paper.

[4] One pertinent example is the reduced phase space $\mathbb{S}^2$ of the Euler top, the freely rotating rigid body.

in the basis $\{|\frac{1}{2},-\frac{1}{2}\rangle,|\frac{1}{2},\frac{1}{2}\rangle\}$.

Coordinates on $\mathbb{S}^2_N$ are dynamical parameters of (2a), while the third control parameter N (see footnote 3) is formal. In the particular example (2), the spherical symmetry results in the conservation of the norm $\|\boldsymbol{J}\|$ of the total angular momentum

$$\boldsymbol{J}=\boldsymbol{N}+\boldsymbol{S},$$

and in constant eigenvalues of (4)

$$\lambda_{1,2}(\boldsymbol{N})=\pm\frac{1}{2}N\ . \tag{5}$$

The slow dynamics is trivial. The degeneracy of the two constant eigenvalues (5) themselves is, in turn, achieved for $N=0$.

2.1.2. *Topologically nontrivial energy bands.* Even though the slow dynamics is trivial, the topology of the parametric semi-quantum system with Hamiltonian (4) is not: just like in the original Berry system with Hamiltonian (1), the two semi-quantum eigenfunction bundles $\Lambda_{1,2}$ over $\mathbb{S}^2_N$ have Chern indices ±1, see Appendix A.1. It is important to uncover how the spectrum of the fully quantum Hamiltonian (2b) reflects this. The SO(3) isotropy of (2b) means that the spectrum is joint with operator $\|\hat{\boldsymbol{J}}\|$, and that the eigenstates are labeled by the respective quantum number J along with N and S. Rewriting (2b) as

$$\hat{H}=\frac{1}{2}\,\hat{\boldsymbol{J}}^2-\frac{1}{2}\left(\hat{\boldsymbol{N}}^2+\hat{\boldsymbol{S}}^2\right),$$

we can see immediately that its spectrum is given by

$$\frac{1}{2}\big(J(J+1)-N(N+1)-S(S+1)\big)$$

and that for given constant N and S, this spectrum has $(2J+1)$-degenerated discrete multiplets corresponding to possible values $|N-S|,|N-S|+1,\dots,N+S$ of J. The spectrum domain $[-(N+1)S,NS]$ is delimited by the energies of multiplets with $J=N-S$ and $N+S$, respectively. So, in particular, the upper and lower multiplets of the $S=\frac{1}{2}$ system consist of $2N+2$ and $2N$ levels, respectively. In the limit $N\gg1$, as detailed further in sec. 2.3.3, the energies of multiplets are pseudo-symmetric with respect to energy 0.

The two multiplets of the $S=\frac{1}{2}$ system are the *energy bands* corresponding to the two semi-quantum eigenvalues $\lambda_{1,2}(N)$. Recall that a multiplet of an isolated system with fixed norm N of angular momentum $\boldsymbol{N}$ has $2N+1$ levels. This number corresponds to the symplectic volume of the underlying classical phase space $\mathbb{S}^2_N$ (plus a quantum correction due to sphere's curvature). The number of levels $\mathcal{N}_{1,2}$ in the two bands of the $S=\frac{1}{2}$ system differs from $2N+1$ by ±1. The difference $2N+1-\mathcal{N}_{1,2}$ equals the values of Chern indices c_1 of $\Lambda_{1,2}$, see Appendix A. This is not coincidental. The bands of the coupled system reflect the nontrivial topology of the semi-quantum description [11, 21].

2.1.3. *Possible deformations.* In order to have the nontrivial slow dynamics and split energy bands, the spherical isotropy of (2) should be removed. At the same

time, there is an option of retaining its time-reversal [5] invariance

$$\mathcal{T} : (\boldsymbol{S}, \boldsymbol{N}) \to (-\boldsymbol{S}, -\boldsymbol{N}), \tag{6}$$

under which *both* angular momenta $\boldsymbol{N}$ and $\boldsymbol{S}$ change sign. In sec. 3 we revisit the simple system [36] with SO(3) broken down to its SO(2) subgroup (axial symmetry) and no $\mathcal{T}$-symmetry, while in sec. 4, we introduce an axially symmetric and $\mathcal{T}$-equivariant deformation of (2). In both cases, we have slow dynamics. The semi-quantum eigenvalues are not constant over the phase space $\mathbb{S}^2_N$, and the latter is foliated with typical constant level sets being periodic orbits $\mathbb{S}^1$. The degeneracy of the bands may still occur locally, at certain points on $\mathbb{S}^2_N$. This brings us to the next section.

2.1.4. *Describing and linearizing the slow dynamics.* The dynamics of a classical slow system on $\mathbb{S}^2_N$ with Hamiltonian $\lambda : \mathbb{S}^2_N \to \mathbb{R}$ can be described using the Poisson algebra so(3) generated by (N_1, N_2, N_3) to obtain the Euler-Poisson equations of motion $\dot{\boldsymbol{N}} = \{\boldsymbol{N}, \lambda(\boldsymbol{N})\}$ and $\dot{N} = 0$. A generic semi-quantum Hermitian 2×2 matrix, such as the one we will encounter in sec. 3, has three real control parameters [41, 1]. This means that the degeneracy of the eigenvalues λ does typically occur in an isolated point $x \in \mathbb{S}^2_N$ and for an isolated value of the third formal control parameter. The local study near x uncovers universal features of quantum, semi-quantum, and classical slow-fast systems with one slow degree of freedom undergoing degeneracy of their semi-quantum eigenvalues. In other words, while such systems may be very different globally, they are equivalent in their behaviour near the isolated degeneracy point. For the semi-quantum systems, the local study of slow dynamics is based on the linearized equations of slow motion at x.

In the subsequent sections, we deform (2) so that the semi-quantum eigenvalues of the deformed systems have generic degeneracies at one or both poles of the slow phase space $\mathbb{S}^2_N$, and we study the respective linearizations. At the north pole with $N_1 = N$, the Poisson bracket $\{N_2, N_3\} = N_1 = N$ suggests that in the most basic, lowest order (linear) approximation, the local symplectic coordinates (q, p) of the chart $\mathbb{R}^2_{q,p}$ at this pole should be chosen as

$$(q, p) = (N_2, N_3)/\sqrt{N} + O((q, p)^2), \tag{7a}$$

while at the origin $(q, p) = 0$ of the chart, we have

$$N_1/N = 1 + O((q, p)^2)\ . \tag{7b}$$

The south pole linearization with $N_1 = -N$ differs in the definition of coordinates (q, p) as summarized below

N_1/N	$\{N_2, N_3\}$	(q, p)	$N_\pm$	N_1
$+1$	$+N$	$(N_2, N_3)/\sqrt{N}$	$a^\mp\sqrt{2N}$	$N - n$
-1	$-N$	$(N_3, N_2)/\sqrt{N}$	$\pm\mathrm{i}\, a^\pm\sqrt{2N}$	$n - N$

(8)

[5] The operation $\mathcal{T}$ has the same effect on the trajectories of the classical system as reversing time in the equations of motion. A more exact terminology, however, may be *momentum reversal*. In classical mechanics, we consider normal and reversing (or reversal) isotropy symmetries of the Hamiltonian function H, depending whether the symplectic form ω remains invariant or covariant [28, 29, 7]. In quantum mechanics, time reversal action on the Hilbert space [42, 6] involves complex conjugation C_* times a unitary transformation. So it can be seen that in the concrete example of Pauli matrices, i.e., for spin-$\frac{1}{2}$ wavefunctions, $\mathcal{T}$ in (6) is realized as $C_* \circ C_2^y$, where C_2^y is rotation by π about axis y (axis 3 in our notation). Although the whole class of reversing symmetries may match Wigner's definition of quantum time-reversal symmetry operation, we like to distinguish our concrete realization of time-reversal proper $\mathcal{T}$ from other reversing symmetries.

with standard oscillator creation-annihilation operators

$$a^\dagger = a^+ := \frac{q - \mathrm{i}p}{\sqrt{2}} = \bar{z}/\sqrt{2} \quad \text{and} \quad a = a^- := \frac{q + \mathrm{i}p}{\sqrt{2}} = z/\sqrt{2}\,. \tag{9}$$

Replacing N_1 and $N_\pm$ in (4) according to (8) gives the spinor forms of (2a) linearized near each pole. Specifically, at the pole with $N_1 \approx N$ we compute

$$\hat{H}\big|_{N_1=N} = \mu\,(2\mu, \sqrt{2}q, \sqrt{2}p)\cdot\hat{\boldsymbol{S}} = \mu \begin{pmatrix} -\mu & a^- \\ a^+ & \mu \end{pmatrix} \text{ with } \mu = \frac{\sqrt{N}}{\sqrt{2}}\,. \tag{10}$$

The linearized spinor form (10) is the most basic universal local representation of any dynamical analogue of the geometric phase setup with Hamiltonian (1).

Linearization is deeply related to the slow phase space localization (footnote 11) of the quantum eigenstates. In the full quantum description, the slow phase space becomes a set of coherent states localized at points on $\mathbb{S}^2_N$ [45], i.e., a set of functions $|N, N\rangle$ with all possible orientations of $\boldsymbol{N}$. Since the slow dynamics for Hamiltonian (2) is trivial, we can associate every state in the $2J+1$ degenerate multiplet of the full quantum system with a specific localized coherent state. Linearization (10) describes what happens to this localized state when formal control parameter μ is varied. In sec. 3 and later, such description will apply to the exceptional *edge* state(s). We like also to note that linearization (10) can be used to calculate the Chern indices c_1 of the semi-quantum eigenfunction bundle $\Lambda_{1,2}$ over $\mathbb{S}^2_{N>0}$. The specific "exceptional point" (see Appendix A.1) where we linearize is coordinate-dependent, but the existence of such point (for any coordinates) reflects the non-triviality of Λ.

2.2. **Dirac oscillator.** The one-dimensional (1D) Dirac oscillator [33], a variation on the theme of the Dirac equation, is the basic dynamical modification of the geometric phase setup with Hamiltonian (1). Using variables (9) and spin $S = \frac{1}{2}$, the semi-quantum Hamiltonian of this system can be written as

$$\hat{H} = \mu \begin{pmatrix} -1 & 0 \\ 0 & 1 \end{pmatrix} + \begin{pmatrix} 0 & a^\dagger \\ a & 0 \end{pmatrix}. \tag{11}$$

The dynamical parameters (q, p) of (11) are symplectic coordinates on the noncompact phase space $\mathbb{R}^2_{(q,p)}$. We notice immediately that for a particular value of μ, this Hamiltonian corresponds to the linearized spin-orbit Hamiltonian (10). In fact, we will see that linearization of the angular momentum system in sec. 3 provides the correspondence for the entire family (11). The eigenvalues of (11)

$$\lambda_{1,2} = \pm\sqrt{n + \mu^2}$$

with classical oscillator action[6]

$$n = \frac{1}{2}(q^2 + p^2) \geq 0,$$

are distinct as long as we stay away from $\mu = q = p = 0$, where they vanish. The additional third formal control parameter μ is needed to have a handle on the sole degeneracy point of $\lambda_{1,2}$. The slow dynamics in $\mathbb{R}^2_{(q,p)}$ consists of motion along the circular orbits with constant n and a single equilibrium at $n = 0$ (and $\mu \neq 0$).

[6]Here again we use the same notation for the classical action I and the oscillator quantum number n, thus simplifying the exact quantum expression $I = n + \frac{1}{2}$ in the limit $n \gg 1$, see footnote 3.

The equations of motions for (q, p) are defined by the Hamiltonian function $\lambda_{1,2}$, cf. sec. 2.1.4.

The major flaw of the previous example in sec. 2.1, is that the degeneracy of its semi-quantum eigenvalues is not generic dynamically because it coincides with the whole slow phase space contracting to one point (a singularity of the slow dynamical system). In particular, this means that the typical energy level redistribution cannot be observed with such parameterization. The Dirac oscillator with Hamiltonian (11) poses no such problem. Its degeneracy occurs at a regular point $n = \mu = 0$.

The indices $c_1 = \pm 1$ of the $\Delta_{1,2}$ bundles over the 2-sphere in the parameter space $\mathbb{R}^3_{(\mu,q,p)}$ encircling the origin give the number of levels which the two energy bands of the full quantum system gain/loose as μ varies through 0. In other words, c_1 gives the number of redistributed levels $\delta\mathcal{N}$. The construction and analysis of $\Delta_{1,2}$ is analogous to that in the original geometric phase setup [38, 43] because the operator form of (11)

$$\hat{H} = 2\mu\,\hat{S}_1 + \sqrt{2}q\,\hat{S}_2 - \sqrt{2}p\,\hat{S}_3 = 2\mu\hat{S}_1 + a_-\hat{S}_+ + a_+\hat{S}_-,$$

where we used cyclic components in (3) and (9), reproduces (1) with

$$\boldsymbol{B} = \left(2\mu, \sqrt{2}q, -\sqrt{2}p\right).$$

The relation between $\boldsymbol{B}$ and the concrete parameters of the system defines the sign in the relation between c_1 and $\delta\mathcal{N}$, see appendices A.2–A.3. On the other hand, comparing the spectra of (10) and (11), these indices can be computed essentially in the same way as for the Λ bundles of the spin-orbit system in sec. 2.1 at constant $N > 0$ which in turn go back to the original geometric phase setup (with $\boldsymbol{B} = \boldsymbol{N}$), see appendix A.1 and A.4. A different calculation, using $\Lambda_{1,2}$ bundles for $\mu < 0$ and $\mu > 0$ with specific boundary conditions [24] yields the same result as "delta-Chern" δc_1 by taking the difference of indices before and after degeneracy for the non-compact classical phase space, see appendix A.3.

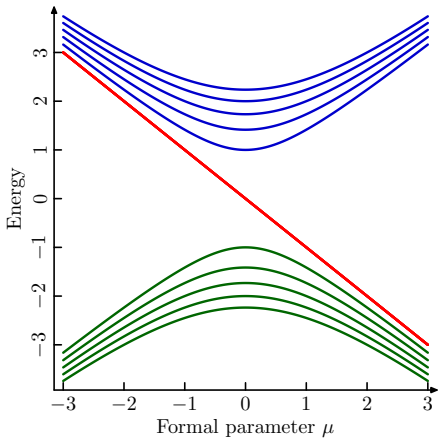

FIGURE 1. Spectrum of the Dirac oscillator with $S = \frac{1}{2}$ as function of formal control parameter μ. The energies of the bulk states (blue and green) and of the edge state (red) are given by (13).

The quantum spectrum of (11) can be computed straightforwardly after we realize that the system has a Lie symmetry with generator $\hat{n} + \hat{S}_1$. Using harmonic

oscillator wavefunctions $|n\rangle$ with $n \in \mathbb{Z}_{\geq 0}$ as a basis in the infinite-dimensional Hilbert space $\mathcal{H}_{\text{slow}}$, we can split $\mathcal{H}_{S=\frac{1}{2}} \times \mathcal{H}_{\text{slow}}$ into a union of two-dimensional subspaces of eigenfunctions of $\hat{n} + \hat{S}_1$ with the same positive half-integer eigenvalue k,

$$\psi_k = \sum_\sigma c_{\sigma,k} \, |S, \sigma\rangle |k - \sigma\rangle \quad \text{with } S = \frac{1}{2}, \ \sigma = \pm\frac{1}{2}, \text{ and } k > 0,$$

and an exceptional sole function

$$\psi_{-\frac{1}{2}} = |\tfrac{1}{2}, -\tfrac{1}{2}\rangle |0\rangle.$$

Replacing (9) for their quantum analogs and recalling the action of operators

$$\hat{a}^\dagger |n-1\rangle = \sqrt{n} \, |n\rangle \quad \text{and} \quad \hat{a}|n\rangle = \sqrt{n} \, |n-1\rangle, \tag{12}$$

we compute the action of (11) on ψ_k and find its eigenvalues

$$\lambda_{-\frac{1}{2}} = -\mu, \quad \lambda_k = \pm\sqrt{\mu^2 + n}, \text{ with } n = k + \frac{1}{2} \in \mathbb{Z}_{>0}. \tag{13}$$

As illustrated in fig. 1, the bulk states ψ_k with $k > 0$ have a pseudo-symmetric spectrum with upper (positive) and lower (negative) bands separated by at least 2. The edge state $\psi_{-\frac{1}{2}}$ passes between the bands when the formal control parameter μ changes sign. We recognize the redistribution phenomenon described in sec. 1.3 and note the universality of the eigenvalue expression (13) which is encountered, with variations and iterations, across many fields, notably in quantum Hall effect [18] and spin-orbit coupling [36]. Multiplying (11) by -1 alternates the "direction" in which the edge state transfers as μ increases through 0 (top down in fig. 1). Parameterizations in sec. 3 and 4 result in the opposite direction, while both directions occur simultaneously in sec. 5 as two copies of (11) with different signs appear in the linearized semi-quantum 4×4 matrix Hamiltonian.

It is also remarkable that for large n, when small quantum corrections to the classical action can be ignored (footnote 6), the quantum bulk energies λ_k match the eigenvalues $\pm\sqrt{\mu^2 + I}$ of the semi-quantum Hamiltonian (11), i.e., the semi-quantum energies. Examining the semiclassical description of the two classical dynamical systems on the slow phase space $\mathbb{R}^2_{q,p}$ whose Hamiltonians are given by the eigenvalues of (11), we can reveal the reasons why the classical action I is quantized as $\tilde{n} + 1$ with $\tilde{n} \in \mathbb{R}_{\geq 0}$, i.e., with a quantum correction of 1. In such systems, phase corrections combine the usual WKB contribution of π and the geometric phase shift [17, Appendix A].

2.3. **Spin-quadrupole system and its dynamical modification.** The quadratic spin-quadrupole interaction Hamiltonian

$$\hat{H} = \hat{\boldsymbol{S}} Q \hat{\boldsymbol{S}} \tag{14}$$

with five-parameter traceless symmetric matrix Q representing *electric quadrupole* is of particular interest to our present study. Being invariant under reversal symmetry

$$\mathcal{T}_S : \hat{\boldsymbol{S}} \to -\hat{\boldsymbol{S}}, \tag{15}$$

Hamiltonian (14) was proposed in [31, 5, 6] as a time-reversal (cf. footnote 5) modification of (1). Our study of $\mathcal{T}$-invariant slow-fast systems is motivated by an attempt to find a dynamical equivalent of the geometric phase analysis in [31, 5, 6].

Drawing the parallel with (1) requires, naturally, to consider states with half-integer spin. For such states, the presence of time-reversal invariance of (14) has one important consequence, known as *Kramers degeneracy* [27, 42]: all quantum

levels of the system form strictly degenerate doublets whose components are related by the symmetry operation (15). It follows that unveiling the spectrum of (14) requires more states in the fast subsystem. The minimal number of these states is four. They can be realized as four spin components with $S = \frac{3}{2}$ which combine into two Kramers degenerate pairs[7]. So just like (1), Hamiltonian (14) for $S = \frac{3}{2}$ has typically two distinct eigenvalues $\lambda_{1,2}(Q)$. These eigenvalues will correspond to the semi-quantum eigenvalues, and comparing to the linear system with Hamiltonian (2), we will have again two quantum bands, but each will now be doubly degenerate.

The matrix of Hamiltonian (14) in the spinor basis

$$\left\{|\tfrac{3}{2},\tfrac{1}{2}\rangle, |\tfrac{3}{2},-\tfrac{1}{2}\rangle, |\tfrac{3}{2},\tfrac{3}{2}\rangle, |\tfrac{3}{2},-\tfrac{3}{2}\rangle\right\} \tag{16}$$

is of the general *quaternionic* form

$$\begin{pmatrix} g & 0 & -c+\mathrm{i}d & a-\mathrm{i}b \\ 0 & g & a+\mathrm{i}b & c+\mathrm{i}d \\ -c-\mathrm{i}d & a-\mathrm{i}b & -g & 0 \\ a+\mathrm{i}b & c-\mathrm{i}d & 0 & -g \end{pmatrix} = \begin{pmatrix} \mathsf{G} & \mathsf{M} \\ \mathsf{M}^\dagger & -\mathsf{G} \end{pmatrix} \tag{17}$$

with eigenvalues

$$\lambda_\pm(Q) = \pm\sqrt{g^2+d^2+c^2+b^2+a^2}$$

of multiplicity 2, and so it follows that the codimension now is 5. In the parameter space $\mathbb{R}^5$, the sole degeneracy point 0 is now surrounded by $\mathbb{S}^4$. The second Chern index c_2 is required to characterize the respective eigenstate bundles $\Delta_{1,2}$. A dynamical extension of (14) can have a slow subsystem with two degrees of freedom and, therefore, four dynamical and one formal control parameter. On the other hand, adding several formal control parameters, we can continue with one slow degree of freedom (sec. 5). Unless the slow phase space is flat, correspondence with [31, 6] will require linearization and local analysis.

2.3.1. *Time reversal symmetries.* In comparison to (2), the spin-quadrupole Hamiltonian (14) has one clear and essential difference: the reversal operation (15) acts *exclusively* on spin components and does not affect the five formal control parameters of the system, the components of the electric quadrupole Q. As a consequence, (14) is quadratic in $\boldsymbol{S}$. On the other hand, our dynamical parameters $\boldsymbol{N}$ are engaged by time reversal (6). This makes us to distinguish reversal operations

$$\mathcal{T}_S : (\boldsymbol{N},\boldsymbol{S}) \to (\boldsymbol{N},-\boldsymbol{S}), \quad \mathcal{T}_N : (\boldsymbol{N},\boldsymbol{S}) \to (-\boldsymbol{N},\boldsymbol{S}), \quad \text{and} \quad \mathcal{T} = \mathcal{T}_S \wedge \mathcal{T}_N$$

generating an order-4 group $Z_2 \times Z_2$. Since (2) and its $\mathcal{T}$-equivariant deformations in sec. 4 are not $\mathcal{T}_S$-invariant, they cannot be dynamical analogues of (14). We should turn to terms of degree 2 in $\boldsymbol{S}$, and furthermore, we can introduce "dynamical quadrupole" Q (sec. 2.3.2) as a symmetric rank-2 tensor constructed of slow variables. Depending on the choice of the slow subsystem and on the particular construction, the resulting system may also come out fully $\mathcal{T}$-invariant, but it will be at least $\mathcal{T}_S$-symmetric.

[7]Another possibility is to consider two fast doublet states, for example a doublet electronic state ^2E or $^2\Pi$ for Jahn-Teller or Renner-Teller systems, respectively

2.3.2. *Dynamical "quadrupole" and spin-quadrupole interaction.* From the components of the standard rank-1 spherical tensor $\boldsymbol{T}^1(\boldsymbol{S})$

$$T^1_0(\boldsymbol{S}) = S_1 \quad \text{and} \quad T^1_{\pm1}(\boldsymbol{S}) = \mp S_\pm \ ,$$

we construct the $\mathcal{T}_S$-invariant tensor of rank 2

$$\boldsymbol{T}^2(\boldsymbol{S}) = \big[\boldsymbol{T}^1(\boldsymbol{S}) \times \boldsymbol{T}^1(\boldsymbol{S})\big]^2$$

with components [44, Appendix 13, eqs.(8–10)]

$$T^2_0(\boldsymbol{S}) = \frac{1}{\sqrt{6}}(3\,S_1^2 - \boldsymbol{S}^2),\ T^2_{\pm1}(\boldsymbol{S}) = \mp\frac{1}{2}[S_1, S_\pm]_+ \quad \text{and} \quad T^2_{\pm2}(\boldsymbol{S}) = \frac{1}{2}S_\pm^2.$$

In the same fashion, we construct $\boldsymbol{T}^2(\boldsymbol{N})$ which models the electric quadrupole Q. In terms of these tensors[8], the closest degree-2 analog of (2) can be written as

$$\hat{H} = \sqrt{5}\left[\boldsymbol{T}^2(\hat{\boldsymbol{S}}) \times \boldsymbol{T}^2(\hat{\boldsymbol{N}})\right]^0 = \left((\hat{\boldsymbol{S}}\cdot\hat{\boldsymbol{N}})^2 - \frac{1}{3}\hat{\boldsymbol{S}}^2\hat{\boldsymbol{N}}^2\right). \tag{18}$$

Like (2), it is spherically symmetric. In the classical limit for $\hat{\boldsymbol{N}}$ and spin-$\frac{3}{2}$ basis (16), the corresponding semi-quantum spin Hamiltonian can be written as a quadratic form (14) whose real symmetric traceless matrix $\mathsf{Q}(\boldsymbol{N})$ has elements[9]

$$Q_{ii} = N_i^2 - \frac{1}{3}N^2 \quad \text{and} \quad Q_{ij} = N_iN_j \ .$$

In the same basis, quantum Hamiltonian (18) is represented as a 4×4 matrix operator whose matrix has quaternionic form (17) with

$$g = \frac{1}{2}\left(N^2 - 3\hat{N}_1^2\right) \tag{19a}$$

and the off-diagonal block

$$\hat{\mathsf{M}} = \frac{\sqrt{3}}{2}\begin{pmatrix}[\hat{N}_1, \hat{N}_+]_+ & \hat{N}_-^2 \\ \hat{N}_+^2 & -[\hat{N}_1, \hat{N}_-]_+\end{pmatrix} \tag{19b}$$

which simplifies into classical expression

$$\mathsf{M} = \frac{\sqrt{3}}{2}\begin{pmatrix}2N_1N_+ & N_-^2 \\ N_+^2 & -2N_1N_-\end{pmatrix}. \tag{19c}$$

So the parameters of the semi-quantum matrix (17) are (19a) with $\hat{N}_1 \to N_1$ and

$$a = \frac{\sqrt{3}}{2}(N_2^2 - N_3^2), \qquad b = -\sqrt{3}\,N_2N_3, \qquad c = -\sqrt{3}\,N_2N_1, \qquad d = \sqrt{3}\,N_3N_1.$$

The system has, as expected, a pair of pseudo-symmetric semi-quantum eigenvalues

$$\lambda_\pm(\boldsymbol{N}) = \pm N^2 \tag{20}$$

with multiplicity 2. The isotropy of (18) becomes the isotropy of (20) with respect to arbitrary rotations of $\boldsymbol{N}$.

---

[8] The only other symmetric powers of degree 2, the rank-0 scalars $\boldsymbol{S}\cdot\boldsymbol{S}$ and $\boldsymbol{N}\cdot\boldsymbol{N}$ are of no interest.

[9] The components of $\boldsymbol{S}$ are labeled in [6] as $(x, y, z) := (2, 3, 1)$.

2.3.3. *Spin-quadrupole and spin-orbit quantum spectra.* We find out the structure of dynamical spin-quadrupole quantum bands that correspond to the semi-quantum eigenvalues (20). It is instructive to do this in comparison to the two bands of the spin-$\frac{1}{2}$ spin-orbit system with Hamiltonian (4) and semi-quantum eigenvalues (5). The linear spin-orbit system with Hamiltonian (2) and the spin-quadrupole system with Hamiltonian (18) are superintegrable. The integrals $\boldsymbol{J} = \boldsymbol{N}+\boldsymbol{S}$, J_1, and energy H are associated with the spherical isotropy group SO(3), its axial subgroup SO(2), and time-independence, respectively. For sufficiently large amplitude of the slow (mechanical) angular momentum $N > S$, with $N \in \mathbb{Z}_{\geq 0}$, the quantum spectrum consists of $2S+1$ multiplets labeled by half-integer $J = N-S, N-S+1, \ldots, N+S$. The even number $2J+1$ of degenerate levels within each multiplet can be further segregated into $J+\frac{1}{2}$ Kramers doublets, each associated additionally with $|J_1| = \frac{1}{2}, \frac{3}{2}, \ldots, J$. Once the strict SO(3) isotropy is broken, this additional classification becomes meaningful.

Both (2) and (18) are traceless and their spectra are centered at $H = 0$. For spin $\frac{1}{2}$ and $\frac{3}{2}$, respectively, these spectra split into two bands of positive ($H > 0$) and negative ($H < 0$) energy. The difference is in the arrangement of J-multiplets with respect to 0, and in the resulting composition of the bands. Being interested in $N \gg S$, we can use a small dimensionless parameter x to express

$$J = N\,(1+x) \quad \text{with } x \in [-\epsilon, \epsilon] \text{ and } \epsilon = \frac{S}{N} \ll 1.$$

Rewriting and renormalizing the linear spin-orbit coupling (2) as

$$h(x) = \frac{\boldsymbol{S}\cdot\boldsymbol{N}}{N^2} = \frac{\boldsymbol{J}^2 - \boldsymbol{N}^2 - \boldsymbol{S}^2}{2N^2} = \frac{x^2}{2} + x - \frac{\epsilon^2}{2},$$

we realize that it is a simple function, essentially linear across its domain,

$$h(x) \approx x + O(\epsilon^2) \quad \text{for } |x| < \epsilon,$$

with single root

$$x_0 = 0 + O(\epsilon^2) \in [-\epsilon, \epsilon].$$

Within the same approach, the spin-quadrupole term (18) equals

$$h(x)^2 - \frac{1}{3}\epsilon^2 = x^2 - \frac{1}{3}\epsilon^2 + O(\epsilon^3).$$

It follows that the energies of J-multiplets in the spectrum of the spin-orbit term increase linearly with J, and so, in particular, the $J = N \pm \frac{1}{2}$ multiplets of the spin $\frac{1}{2}$ system are opposite in energy $\pm x\,N^2$. On the other hand, the spectrum of the spin-quadrupole term is quadratic in J, and furthermore, the energies are negative for $|x| < \epsilon/\sqrt{3}$. So in the particular case of spin $\frac{3}{2}$, the two multiplets with $J = N \pm \frac{1}{2}$ and $x = \pm\epsilon/3$ have negative energies, while those with $J = N \pm \frac{3}{2}$ have positive energies. To acknowledge their additional internal structure, we call the two bands of the spin-$\frac{3}{2}$ system *superbands*, implying that a superband is constituted by several subbands or multiplets.

Knowing the values of J for the multiplets within each superband, we can easily find the number of states with given $|J_1|$ required to constitute these multiplets. So in particular for $S = \frac{3}{2}$, we can see that typically, for small $|J_1| \leq N - \frac{3}{2}$, each band has two such states, one per multiplet. For larger $|J_1| = N - \frac{3}{2} + 1, \ldots, N + \frac{3}{2}$, i.e., $N - \frac{1}{2}$, $N + \frac{1}{2}$, and $N + \frac{3}{2}$, we have 3, 2, and one single doublet state, respectively. When the number of doublets is even, i.e., for $|J_1| = N + \frac{1}{2}$, they split evenly between the bands. Otherwise, the lower band has one extra doublet state with

$|J_1| = N + \frac{3}{2} - 2$ required to complete the multiplet with $J = N - \frac{1}{2}$, and the upper band takes the sole doublet with maximal $|J_1| = N + \frac{3}{2}$. We come to the following proposition.

Proposition 1 (spectrum of (18))**.** *When $N \gg S$, the upper and lower superbands (bands) of the spin-$\frac{3}{2}$ system with Hamiltonian (18) are formed by $J = N \pm \frac{3}{2}$ and $J = N \pm \frac{1}{2}$ multiplets, respectively. The superbands have an equal number $2N + 1$ of Kramers quantum level doublets labeled by the value of $|J_1|$. In each superband, the number of doublets with $|J_1|$ other than $N + S$ and $N + S - 2$ is the same. The lower band has one extra doublet state with $|J_1| = N + S - 2$, while the upper band takes the sole doublet with maximal $|J_1| = N + S$ as part of its $J = N + S$ multiplet.*

The exact quantum spectrum of (18) for concrete N and S can be, of course, obtained if we use quantum expressions for the eigenvalues of all operators in $h(x)$. Thus we should replace $\boldsymbol{J}^2$ by $N^2(1+x)^2 + N(1+x)$. Alternatively, we can apply the Wigner-Eckart theorem as detailed by eq. (5.71) of [44, chap. 5.4]

$$\lambda(J) = (-1)^{S+N+J} \begin{Bmatrix} S & N & J \\ N & S & 2 \end{Bmatrix} \langle S \| \boldsymbol{T}^2(\boldsymbol{S}) \| S \rangle \, \langle N \| \boldsymbol{T}^2(\boldsymbol{N}) \| N \rangle \tag{21}$$

with reduced matrix elements of $\boldsymbol{T}^2$ in eq. (35) of [44, Appendix 13]. Analyzing the sign in (21), we confirm the statement of proposition 1 about the number of states in the bands of the spin-$\frac{3}{2}$ system. It may also be instructive to see how (21) converges to just two distinct values (20) when $S = \frac{3}{2}$ and $S/N \to 0$.

The seeming triviality of the superbands of the spin-$\frac{3}{2}$ system does also merit a comment. In fact, the individual subbands in these superbands are not trivial. The corresponding eigenstate "superbundles" Λ^+ and Λ^- representing upper and lower superbands consist of two bundles representing the subbands and corresponding to the individual semiquantum eigenstates. The bundles and the subbundles are not trivial, but indices for each superbundle sum up to 0. See more in sec. 5.3.

3. **Original family without time-reversal symmetry.** The system with the spin-orbit coupling Hamiltonian (2) has one essential shortcoming: its degeneracy point $\{N = 0\}$ happens to be the singularity of its slow dynamical system, whose phase space $\mathbb{S}^2_N$ contracts to one point. We need a different formal control parameter γ, such that the topology of the phase space is not affected by its variation, while N can simply be fixed.

Additionally, we like to break the isotropy of (2) in order to have regular dynamics on $\mathbb{S}^2_N$ and a nondegenerate spectrum within the energy bands. As suggested in [36], this can be most trivially achieved by combining (2) with a one parameter $\boldsymbol{N}$-independent sub-family of (1). Without any loss of generality, we can add $\hat{S}_1$ times a γ-dependent factor $B(\gamma)$. It follows that we are bound to have two limits, one of *coupled momenta* with dominating Hamiltonian (2a), the other of *uncoupled momenta* with Hamiltonian (1) and $\boldsymbol{B} = (1, 0, 0)$. These limits and the correlation diagram connecting them are represented in fig. 2.

The coupled limit has already been analyzed in sec. 2.1. The uncoupled system is rather simple. The semi-quantum eigenstates with energies $\lambda_{1,2} = \pm\frac{1}{2}$ are spin states $|-\frac{1}{2}\rangle$ and $|+\frac{1}{2}\rangle$ that remain unchanged over the parameter space $\mathbb{S}^2_N$, thus forming two trivial line bundles over $\mathbb{S}^2_N$ with $c_1 = 0$. The quantum system consists of two multiplets (bands) with energies $\lambda_{1,2}$. Each multiplet has $2N + 1$ degenerate levels, the normal degeneracy of an isolated (uncoupled) quantum rotator with

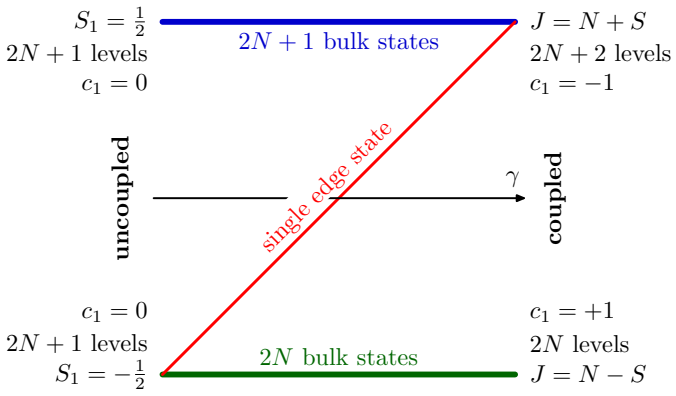

FIGURE 2. Correlation diagram of the deformed spin-orbit system with spin $S = \frac{1}{2}$ and $N \gg S$ as function of formal coupling control parameter γ. Bold solid lines represent the energies of the bulk states (blue and green) and the edge state (red). When the value of γ varies, one single state (edge) changes bands, while all other states (bulk) remain within the same band.

constant N. We conclude that in the simplest case (fig. 2), going from one limit to the other should involve a transfer of a single edge state. The Chern indices for the $\Lambda_{1,2}$ bundles over $\mathbb{S}^2_N$ for different values of γ can be defined and computed similarly to those in the original geometric phase setup with (1) as discussed across secs. 1.1, 1.3, and 2.1 and Appendix A.1. This allows to indicate c_1 in fig. 2 without any special computations which are relegated to Appendix A.5. The change δc_1 corresponds to one state being gained/lost by the respective bands.

3.1. **Spin-orbit coupling in the presence of magnetic field.** The parametric system with two coupled angular momenta $\boldsymbol{N} = (N_1, N_2, N_3)$ and $\boldsymbol{S} = (S_1, S_2, S_3)$ of constant respective lengths $N := \|\boldsymbol{N}\|$ and $S := \|\boldsymbol{S}\|$ (footnote 3) exhibiting the redistribution phenomenon in fig. 2 was suggested in [36] and was further analyzed in [37, 21]. We associate $\boldsymbol{N}$ and $\boldsymbol{S}$ with "slow" mechanical angular momentum and "fast" spin subsystem, respectively. The Hamiltonian

$$\hat{H}_\gamma = (1-\gamma)\frac{\hat{S}_1}{\|\boldsymbol{S}\|} + \gamma\,\frac{\boldsymbol{N}\cdot\hat{\boldsymbol{S}}}{\|\boldsymbol{N}\|\|\boldsymbol{S}\|}, \qquad \text{for } S = \tfrac{1}{2} \text{ and } \gamma \in [0,1]. \tag{22}$$

can represent two coupled angular momenta in the presence of magnetic field. Both the spin-orbit coupling constant α and the norm B of the magnetic field $\boldsymbol{B} = B(1,0,0)$ depend on the formal control parameter γ so that at the boundaries of the parameter domain, we reach the limits of uncoupled ($\gamma = 0$) and coupled ($\gamma = 1$) momenta occurring in fig. 2. Exploiting conservation of $N > 0$ and $S > 0$, we scale the terms in (22) to make the results dimensionless and concise. Using quantum numbers $N > 0$ and $S > 0$ as scaling constants (footnote 3) simplifies expressions further as some factors cancel out.

The Hamiltonian (22) has nontrivial Lie isotropy group $\mathbb{S}^1$ constituted by simultaneous rotations of $\boldsymbol{N}$ and $\boldsymbol{S}$ about axis 1 (also called axis z elsewhere). The corresponding conserved quantity is the combined projection

$$J_1 = N_1 + S_1 \tag{23}$$

of $\boldsymbol{N}$ and $\boldsymbol{S}$ on the axis of symmetry. One of the consequences of this symmetry is that the classical analog system is integrable, another consequence is the factorization of the matrix of the quantum Hamiltonian $\hat{H}$ into one- and two-dimensional blocks. This all is very similar to the Dirac oscillator symmetry with generator $\hat{n}+\hat{S}_1$ (sec. 2.2).

3.1.1. *Semiquantum energies.* The semi-quantum (spinor) matrix representation of Hamiltonian (22)

$$\hat{H}_\gamma = (1-\gamma)\begin{pmatrix}-1 & 0\\ 0 & 1\end{pmatrix} + \frac{\gamma}{N}\begin{pmatrix}-N_1 & 0\\ 0 & N_1\end{pmatrix} + \frac{\gamma}{N}\begin{pmatrix}0 & N_+\\ N_- & 0\end{pmatrix} \tag{24}$$

is obtained similarly to (4). It commutes with

$$\hat{J}_1 = \begin{pmatrix}N_1-\frac{1}{2} & 0\\ 0 & N_1+\frac{1}{2}\end{pmatrix} \tag{25}$$

and its eigenvalues

$$\lambda_{1,2} = \pm\sqrt{1-2\gamma\,(1-\gamma)\,(N-N_1)\,N^{-1}} \in \left[\pm|1-2\gamma|, \pm 1\right] \tag{26}$$

are axially symmetric simplest Morse functions on $\mathbb{S}^2_N$ with just one mandatory pair of stationary points, a maximum and a minimum. The action of axial symmetry on $\mathbb{S}^2_N$ (rotation about axis N_1) has two isolated critical points with extremal values $(\pm N)$ of N_1 (poles) at which semi-quantum energies (26) reach their critical values. These energies become degenerate at the south pole $(N_1, N_2, N_3) = (-N, 0, 0)$ when $\gamma = 1/2$. The degeneracy of $\lambda_{1,2}$ has the generic local form of a conical intersection of two 2-surfaces. The eigenfunctions corresponding to $\lambda_{1,2}$ form two nontrivial bundles $\Delta_{1,2}$ over a 2-sphere surrounding the isolated degeneracy point in the parameter space (γ, N_2, N_3). These bundles have indices[10] $c_1 = \pm 1$, see Appendix A.5. We can also consider bundles $\Lambda_{1,2}(\gamma)$ with $\gamma \neq \frac{1}{2}$ of the same eigenvectors over the base $\mathbb{S}^2_N$. In this case, the bundles are trivial ($c_1 = 0$) when $\gamma \in [0, \frac{1}{2})$ and nontrivial ($c_1 = \pm 1$) when $\gamma \in (\frac{1}{2}, 1]$. Such bundles represent the energy bands of the quantum system (fig. 3) and the index change reflects the redistribution of one energy level between the bands (fig. 2).

On the slow phase space $\mathbb{S}^2_N$, the classical motion goes along the orbits of the axial symmetry which are constant level sets of N_1. In sec. 3.2 we relate these sets to the orbits of the Dirac oscillator (sec. 2.2). The system has two elliptic equilibria at the poles $\{|N_1| = N\}$. All other orbits are generic $\mathbb{S}^1_{N_1}$ circles

$$\{N_2^2 + N_3^2 = N^2 - N_1^2,\ |N_1| < N\} \subset \mathbb{S}^2_N.$$

The slow dynamics under (24) can be described using variables (N_2, N_3) if we distinguish additionally the south ($N_1 < 0$) and the north ($N_1 > 0$) hemispheres (charts). The $\mathbb{S}^1_{N_1}$ orbits lie in the base of both the $\Lambda_{1,2}$ and the $\Delta_{1,2}$ bundles. In either case, they are associated with a nonzero geometric phase (cf sec. 2.1). The

[10] As pointed out in sec. 1.4, all bundle constructions and index computations for the systems in sec. 3 come back to those in the original plain setup with Hamiltonian (1). Specifically, substituting

$$N_1 = -\sqrt{N^2 - N_2^2 - N_3^2}, \quad \gamma = \frac{1}{2} - \frac{\mu}{4N}, \quad \text{and} \quad \frac{1}{2NS}\,(\mu, N_2, N_3) =: (B_1, B_2, B_3)$$

into Hamiltonian (22), and Taylor expanding to the principal order in $\boldsymbol{B}$ result in (1) which we analyze in the standard way [38, 43]. All local bundles Δ, including those discussed in sec. 2.2 (with noncompact slow phase space $\mathbb{R}^2_{q,p}$), 4, and 5 can be treated similarly. The same applies to any bundle Λ over $\mathbb{S}^2_N$, starting with sec. 2.1 where we identify $\boldsymbol{N}$ with control parameters $\boldsymbol{B}$ of (1).

latter can be, in particular, seen as the origin of a specific additional contribution in the semi-classical quantization of slow dynamics (sec. 3.1.2).

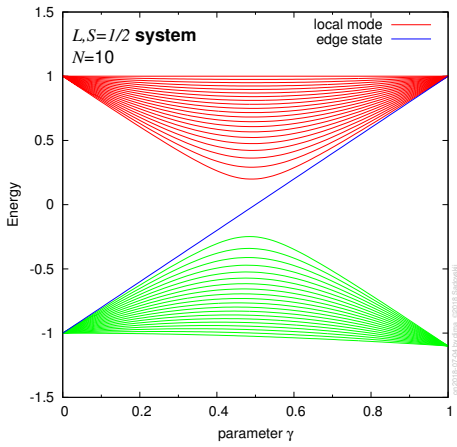

FIGURE 3. Spectrum of the $N, S = \frac{1}{2}$ system (two coupled angular momenta of conserved lengths) with Hamiltonian $\hat{H}_\gamma$ (22) as function of parameter γ (scaled magnetic field strength). Green and red solid lines represent the "bulk" states of the lower and upper band (multiplet); blue solid line marks the energy of the single "edge" state redistributed at $\gamma = \frac{1}{2}$.

3.1.2. *Edge and bulk states of the quantum spectrum.* The full quantum system is solvable on finite Hilbert subspaces $\mathcal{H}_j$ spanned by eigenfunctions ψ_j of operator $\hat{J}_1$ with the same eigenvalue j. Using spin functions $|\frac{1}{2}, \pm\frac{1}{2}\rangle$ and spherical functions $|N, k\rangle = Y_{N,k}$ with $|k| = 0, 1, \ldots, N$, we construct uncoupled basis spinor functions

$$\psi_j = a|\tfrac{1}{2}, -\tfrac{1}{2}\rangle|N, k\rangle + b|\tfrac{1}{2}, +\tfrac{1}{2}\rangle|N, k-1\rangle =: \begin{bmatrix} a \\ b \end{bmatrix}_j \text{ with } \bar{a}a + \bar{b}b = 1$$

for all values of $k \in \mathbb{Z}$ and $j = k - \frac{1}{2}$ such that $|j| < N + \frac{1}{2}$, while for the exceptional extremal values $j = \pm(N + \frac{1}{2})$ we have two single functions

$$\psi_{-N-\frac{1}{2}} = |\tfrac{1}{2}, -\tfrac{1}{2}\rangle|N, -N\rangle \text{ and } \psi_{N+\frac{1}{2}} = |\tfrac{1}{2}, \tfrac{1}{2}\rangle|N, N\rangle.$$

The eigenvalues of the action of quantum Hamiltonian $\hat{H}_\gamma$ (22) on $\mathcal{H}_j$ with regular j

$$\lambda_j = \pm\sqrt{1 + 2\gamma\,(1-\gamma)\,\frac{j-N}{N} + \gamma^2\frac{4N+1}{4N^2}} - \frac{\gamma}{2N}, \quad \text{where } |j| < N + \tfrac{1}{2}, \tag{27}$$

represent bulk eigenstates belonging to different bands. The exceptional functions $\psi_{\pm(N+1/2)}$ are eigenfunctions of $\hat{H}_\gamma$ with eigenvalues

$$\lambda_\pm := \lambda_{\pm(N+1/2)} = \pm(1-\gamma) + \gamma.$$

So $\lambda_+ \equiv 1$ remains constant, while $\lambda_- = 2\gamma - 1$ increases linearly from -1 to 1 as γ sweeps through the interval $[0, 1]$.

Figure 3 shows the spectrum of the system. Considering the localization patterns of the exceptional states, their energies $\lambda_\pm$ can be easily understood[11]. The states $|N, \pm N\rangle$ correspond to coherent states localized maximally around the poles $N_1 = \pm N$ of the slow phase space $\mathbb{S}^2_N$, i.e., near the equilibria of the slow system. Their Wigner distribution has a small "round shape" with a maximum at the respective pole and a near Gaussian profile similar to that of the harmonic oscillator ground state. The eigenfunction ψ_+ is localized near the $N_1 = N$ pole, opposite to the one where the degeneracy occurs. It is the state which is most distant from the conical intersection point and its energy is not affected by the interaction between (coupling of) the bands. On the other hand, the eigenfunction ψ_- is localized right where bad things happen. It represents the edge state. This state is critically affected by slow-fast separation breakdown which occurs when $\gamma \approx \frac{1}{2}$.

3.2. **Linearization at the degeneracy point.** The conical intersection of the semi-quantum energy surfaces $\lambda_{1,2}(\boldsymbol{N}; \gamma)$ of the original system with Hamiltonian (22) occurs at the $N_1 = -N$ pole on the slow phase space $\mathbb{S}^2_N$. Near this pole, when γ approaches its critical value $\frac{1}{2}$, the dynamics accelerates, the slow-fast separation breaks down locally, and the exceptional highly localized (see footnote 11) quantum state ψ_- gets redistributed. We linearize our system near this point following the outline in sec. 2.1.4, and move to the tangent plane $\mathbb{R}^2_{q,p} = T_{N_1=-N}\mathbb{S}^2_N$ which serves as a symplectic chart of $\mathbb{S}^2_N$ with local symplectic coordinates (q, p).

In the basic approximation of eq. (8), the Hamiltonian (24) becomes

$$\hat{H}_\gamma\big|_{N_1 \approx -N} = (1 - 2\gamma) \begin{pmatrix} -1 & 0 \\ 0 & 1 \end{pmatrix} + \gamma \frac{\sqrt{2}}{\sqrt{N}} \begin{pmatrix} 0 & \mathrm{i}a^+ \\ -\mathrm{i}a^- & 0 \end{pmatrix}. \tag{28}$$

Rescaling the energy, reparameterizing with new formal control parameter

$$\mu = \frac{1 - 2\gamma}{\gamma} \frac{\sqrt{N}}{\sqrt{2}},$$

and adjusting the phase of one of the basis functions turn it into the standard Hamiltonian (11) of the one-dimensional (1D) Dirac oscillator [33], see sec. 2.2. The two semi-quantum eigenvalues of (11) and (28) are functions on the flat noncompact slow phase space $\mathbb{R}^2_{q,p}$. It follows that $\mu \to \infty$ makes the two bands of the Dirac oscillator completely uncoupled. While the uncoupled limit is unreachable for finite values of formal control parameter μ, near $\mu = 0$ and $\gamma = \frac{1}{2}$, the two respective systems exhibit the same redistribution phenomenon and their local eigenstate bundles $\Delta_{1,2}$ (cf. footnote 10) over a sphere $\mu^2 + n = \text{const}$ are isomorphic.

Linearization (28) allows making the correspondence of the systems with Hamiltonians (24) and (11) explicit and complete. The 1:1 correspondence of the harmonic oscillator wavefunctions $|n\rangle$ of the noncompact slow system and the angular momentum wavefunctions $|N, k\rangle$ with $k = j + \frac{1}{2}$ can be readily established after noting that the oscillator ground state $|0\rangle$ corresponds to the coherent state $|N, -N\rangle$ localized at the south pole, and that the number of nodes of the excited states $|n\rangle$ equals the number of nodes in the radial direction (footnote 11)). This suggests $n = -N + k$. Expanding N_1 near $-N$ to order $O((q, p)^4)$ gives the same result, see (8). Furthermore, through the equivalence of the two first integrals, J_1 with

[11] Localization in the phase space $\mathbb{S}^2_N$ corresponds to the orientation probability of $\boldsymbol{N}$. The latter is given by the Wigner distribution W of the eigenstates and has no relation to the angular probability distribution used commonly to represent spherical functions, see, for example, [30] and the discussion in [11, 16].

value j and $n + S_1$ with value k', we come to the correspondence of the respective Hilbert subspaces $\mathcal{H}_j$ and $\mathcal{H}_{k'}$, and subsequently—to the equivalence of the edge states and the first N bulk states of the two systems. For $k' > N$ we loose nodal correspondence, and of course, beyond $k' = 2N$, the states of the Dirac oscillator find no analogue in the spin-orbit system. The correspondence can be followed as well at the semiquantum level where the circular orbits $\mathbb{S}^1_{N_1} \subset \mathbb{S}^2_N$ with $N_1 < 0$ map to harmonic oscillator trajectories in $\mathbb{R}^2_{q,p}$ with sufficiently small n. In other words, the orbits of the Lie symmetries of the two slow classical systems, the axial symmetry and the oscillator symmetry, respectively, are diffeomorphic for $n \leq N$. And finally, at the classical level, both systems exhibit the same kind of nontrivial Hamiltonian monodromy [37].

4. **Spin-orbit systems with time-reversal symmetry.** Unless in the presence of an external magnetic field, molecular and atomic systems are invariant with respect to time reversal (6), see footnote 5. The system with Hamiltonian (22) is not $\mathcal{T}$-invariant for $\gamma < 1$. We like to find a $\mathcal{T}$-invariant system which exhibits similar qualitative behaviour with respect to the variation of a single control parameter. Specifically, we want this system to have two bands of approximately $2N$ states each for all typical values of parameter $\alpha \in [-1, 1]$, and we like a redistribution of (few) levels between the bands to occur at the isolated critical value $\alpha = 0$.

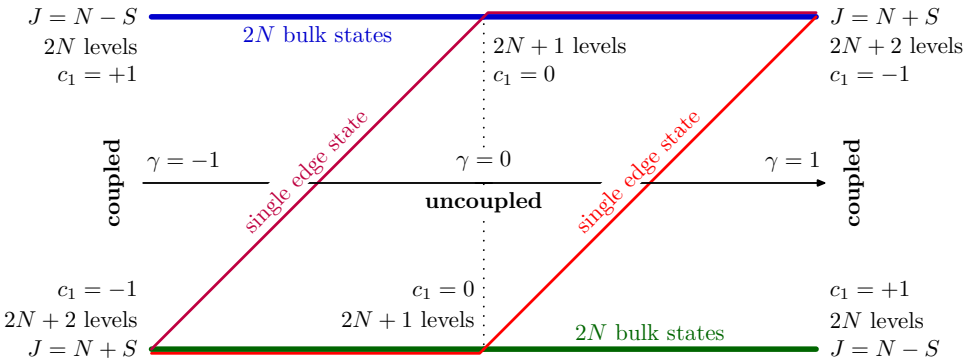

FIGURE 4. Correlation diagram of the deformed spin-orbit system with Hamiltonian (29), spin $S = \frac{1}{2}$, and $N \gg S$ as function of formal coupling control parameter γ. In comparison to the diagram in fig. 2, the domain of γ is extended from $[0, 1]$ to $[-1, 1]$; the $\gamma > 0$ parts of both diagrams are identical. The value 0 of γ corresponds to the uncoupled system (two bands of equal number of states), while the values -1 and $+1$ correspond to the coupled spin-orbit system with negative and positive coupling Hamiltonian (2). Bold solid lines represent the energies of the bulk states (blue and green) and the edge states (red). When the value of γ varies, two single states (edge) change bands, while all other states (bulk) remain within the same bands.

Hamiltonian (22) becomes $\mathcal{T}$-invariant in the limit $\gamma \to 1$ which is discussed in detail in sec. 2.1. Its upper and lower $2(J + 1)$-degenerate bands with $J = N + \frac{1}{2}$ and $J = N - \frac{1}{2}$, respectively, include $2N + 2$ and $2N - 2$ levels (see fig. 2). If we

reparameterize (22) so that the new Hamiltonian

$$\hat{H}^*_\gamma = (1-|\gamma|)\,\frac{S_1}{\|\boldsymbol{S}\|} + \gamma\,\frac{\boldsymbol{N}\cdot\boldsymbol{S}}{\|\boldsymbol{N}\|\|\boldsymbol{S}\|}, \qquad \text{with } S=\frac{1}{2} \text{ and } |\gamma|\le 1, \tag{29}$$

is identical to (22) for $\gamma > 0$ and has the extended parameter domain $[-1,1]$, we get another $\mathcal{T}$-invariant limit with $\gamma = -1$. In comparison to $\gamma = 1$, the upper band corresponds now to $J = N - \frac{1}{2}$ and has fewer levels. In the spectrum of (29), when γ decreases on the interval $\gamma \in [0,1]$, i.e., as we follow fig. 2 and 3 right to left, one state is redistributed top down at $\gamma = +\frac{1}{2}$. For $|\gamma| < \frac{1}{2}$, both bands have $2N+1$ states. Subsequently, when γ decreases further on the interval $\gamma \in [0,-1]$, one additional state is redistributed top down at $\gamma = -\frac{1}{2}$. This process is represented by the correlation diagram in fig. 4. The combination of the two one-state redistributions connects one $\mathcal{T}$-limit to another by passing through a family systems with Hamiltonian (29) which are not $\mathcal{T}$-invariant.

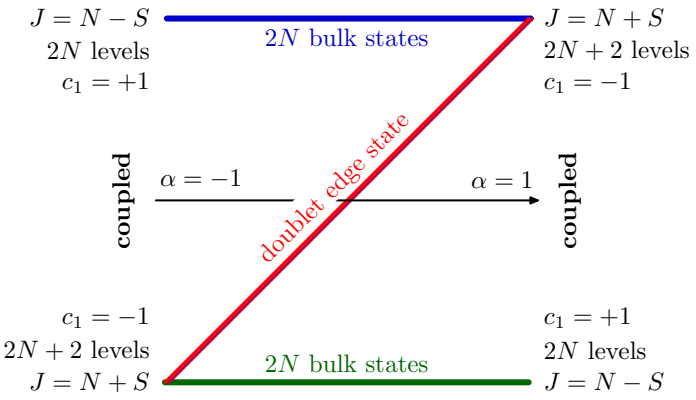

FIGURE 5. Correlation diagram of the spin-orbit system with the conjectured $\mathcal{T}$-equivariant deformation, spin $S = \frac{1}{2}$, and $N \gg S$ as function of formal coupling control parameter α. In comparison to the diagram in fig. 4, the $[-\frac{1}{2}, \frac{1}{2}]$ part of the domain of γ is shrunk to 0, while the endpoints of the two diagrams are identical. There is no uncoupled system, the values -1 and $+1$ of α correspond to the coupled spin-orbit system with isotropic negative and positive coupling Hamiltonian (2). Bold solid lines represent the energies of the bulk states (blue and green) and one Kramers doublet edge state (red).

It can be conjectured that another passage exists entirely within the class of $\mathcal{T}$-invariants. In such a case, since all quantum states form Kramers degenerate doublets when the norm of the total angular momentum J is half-integer, specifically, when $S = \frac{1}{2}$ and $N \in \mathbb{Z}_{>0}$, the two edge states in fig. 4 must become one doublet state. As illustrated in fig. 5, this single doublet state is redistributed, while all other states (bulk) remain within their bands. Mapped between themselves by the $\mathcal{T}$ symmetry operation, the two states in the edge doublet are localized at the opposite points on the slow phase space $\mathbb{S}^2_N$. So, if the axial symmetry is preserved, they will be pole-localized coherent states $\psi_{\pm J_1}$ with $|J_1| = N + S$ which we have already encountered in sec. 3.1.2.

4.1. **The family of $\mathcal{T}$-invariant Hamiltonians.** We construct explicitly the conjectured $\mathcal{T}$-equivariant connection of the $\alpha = \gamma = \pm 1$ limits of Hamiltonian (29) as a one parameter family. The reparameterized spherically symmetric spin-orbital coupling term (2)

$$\alpha \frac{\boldsymbol{N} \cdot \boldsymbol{S}}{\|\boldsymbol{N}\|\|\boldsymbol{S}\|}, \quad \text{with } S = \frac{1}{2} \text{ and } \alpha \in [-1, 1],$$

defines the two limits with $\alpha = \pm 1$ and is the principal term of the family. However, with only this term, the two bands collapse for $\alpha = 0$ and then change places for $\alpha \neq 0$. We must introduce another $\mathcal{T}$-invariant term with a fixed parameter $0 < \varepsilon < 1$ in order to recover most of the band structure (bulk states) for all values of α. This additional ε-term breaks the spherical symmetry of (2).

Similarly to the systems with Hamiltonians (22) and (29), our $\mathcal{T}$-invariant family of systems can retain the global axial symmetry with first integral J_1. It can be argued that an approximate $\mathbb{S}^1$ symmetry action on the slow (classical) space can always be introduced and exploited near an isolated degeneracy point of the two semi-quantum eigenvalues. In the presence of this symmetry, the redistributed edge states are strongly localized (footnote 11) near the symmetry axis. In our $\mathcal{T}$-invariant spin-$\frac{1}{2}$ system with integer N, the edge states correspond to the states $\psi_{\pm|J_1|}$ with maximal $|J_1| = N + \frac{1}{2}$ (see sec. 3.1.2) now forming one Kramers doublet. The presence of the global $\mathbb{S}^1$ symmetry, if possible, will greatly simplify the analysis without any loss of generality.

Since any additional terms should not affect the redistribution of the edge state doublet (fig. 5), we may require these terms to be function of $\boldsymbol{S}$ and N_2, N_3 (or $N_\pm$) only. Such terms can be called "equatorial" because they vanish, or become maximal when $\boldsymbol{N}$ is aligned with, or is orthogonal to axis 1, respectively, i.e., when $\boldsymbol{N} \cdot \boldsymbol{e}_1 = N$ or $\boldsymbol{N} \cdot \boldsymbol{e}_1 = 0$.

Under the action of $\mathcal{T}$, the equator becomes the critical set on the slow (classical) space $\mathbb{S}^2_N$. The "equatorial" states with $N_1 \approx 0$ are the most distant from the edge states $\psi_\pm$, and we can expect the critical value λ_{crit} of the semi-quantum eigenvalue $\lambda(\boldsymbol{N}, \alpha)$ on the equator to mark the absolute maximum and minimum energy of the "bulk" states in the upper and lower bands (multiplets) with large $|\alpha| \approx 1$. As a consequence, in order to remain the absolute maximum and minimum in the transition region, λ_{crit} should be essentially quadratic in α for small $|\alpha/\varepsilon| \ll 1$.

In summary, the requirements on the potential ε-term(s) are: (i) to preserve, if possible, the SO(2) symmetry, (ii) to have the equatorial behaviour (on the slow space), and (iii) to provide the essential quadratic dependence of the critical equatorial energy on α. These requirements can be reformulated somewhat differently and more stringently by demanding the quantum spectrum of the ε-term alone (i.e., for $\alpha = 0$) to be pseudo-symmetric with two edge states remaining at zero energy and with equal numbers of bulk states of positive and negative energy. This means that the two eigenvalues of the corresponding semiquantum system with spin $\frac{1}{2}$ are also pseudo-symmetric and have degeneracy points at the poles.

Considering all bilinear (and so necessarily $\mathcal{T}$-invariant) forms in $\boldsymbol{N}$ and $\boldsymbol{S}$, we come up with two Hermitian axially symmetric terms other than (2)

$$\frac{1}{2}\big(N_+ S_- + N_- S_+\big) = \boldsymbol{N} \cdot \boldsymbol{S} - N_1 S_1 \quad \text{and} \tag{30a}$$

$$\frac{\mathrm{i}}{2}\big(N_- S_+ - N_+ S_-\big) = (\boldsymbol{N} \wedge \boldsymbol{S}) \cdot \boldsymbol{e}_1 \ . \tag{30b}$$

Of these, only (30b) satisfies the above conditions, while the trivial choice (30a) does not conform to requirement (iii). On the same Hilbert space as in (4), the Hamiltonian

$$\hat{H}^1_\alpha = \alpha \, \frac{\boldsymbol{N}\cdot\boldsymbol{S}}{\|\boldsymbol{N}\|\|\boldsymbol{S}\|} - \mathrm{i}\,\varepsilon \, \frac{N_+S_- - N_-S_+}{2\,\|\boldsymbol{N}\|\|\boldsymbol{S}\|} \ , \tag{31}$$

with $\|\boldsymbol{S}\| = S = \frac{1}{2}$, $\alpha \in [-1,1]$, and small $\varepsilon \neq 0$, has spinor representation

$$\hat{H}^1_\alpha = \frac{\alpha}{N}\begin{pmatrix} -N_1 & 0 \\ 0 & N_1 \end{pmatrix} + \frac{\alpha}{N}\begin{pmatrix} 0 & N_+ \\ N_- & 0 \end{pmatrix} - \mathrm{i}\,\frac{\varepsilon}{N}\begin{pmatrix} 0 & N_+ \\ -N_- & 0 \end{pmatrix} \ . \tag{32}$$

Its semi-quantum eigenvalues

$$\pm\sqrt{\varepsilon^2\sin^2\theta + \alpha^2} \tag{33}$$

have critical points at the poles with latitudinal angle $\theta = 0, \pi$ and the equatorial critical set $\mathbb{S}^1 = \{\theta = \pi/2\}$. The corresponding critical values of semi-quantum energies $\lambda_{1,2}(\boldsymbol{N},\alpha)$ with $\theta = 0,\pi$ and $\theta = \pi/2$ are shown by dotted lines in fig. 6. The poles belong to the same critical 2-point orbit of the $\mathrm{SO}(2) \wedge \mathcal{T}$-group action on $\mathbb{S}^2_N$ and the energy at both poles has the same critical value $\pm|\alpha|$. This value describes the behaviour of the edge states localized (footnote 11) near the poles. The equatorial energy $\pm\sqrt{\varepsilon^2+\alpha^2}$ has the desired property (iii). This confirms the family (31–32).

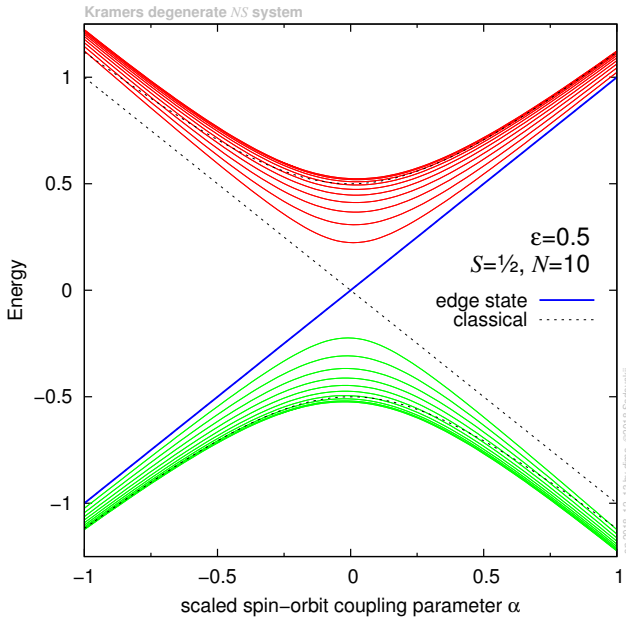

FIGURE 6. Spectrum of the $N, S = \frac{1}{2}$ system (two coupled angular momenta of conserved lengths) with $\mathcal{T}$-invariant Hamiltonian (31) as function of scaled spin-orbit coupling parameter α. Each solid line represents a Kramers doublet quantum state. Energies of the bulk states (red and green solid lines) are given by (34), while the solid blue line represents the edge state. Dotted lines indicate critical values of the semi-quantum energies (33).

4.1.1. *Quantum spectrum of the $\mathcal{T}$-invariant family.* We analyze the spectrum of (31) using its spinor representation (32). Following the approach in sec. 3.1.2, specifically see (24), we compute the action of (32) on each Hilbert subspace $\mathcal{H}_j$ with $|j| < N + \frac{1}{2}$ and $k = j + \frac{1}{2} \in \mathbb{Z} \cap (-N, N+1)$. This gives the energies

$$\lambda_j = -\frac{\alpha}{2N} \pm \frac{1}{N}\sqrt{\alpha^2 j^2 + R_j^2(\alpha^2 + \varepsilon^2)} \tag{34}$$

of the bulk states with

$$R_j := \sqrt{(N+k)(N-k+1)} = \sqrt{\left(N+j+\tfrac{1}{2}\right)\left(N-j+\tfrac{1}{2}\right)} > 0. \tag{35}$$

Since R_j is invariant with respect to sign flipping $j \mapsto -j$, we observe that each $\lambda_{\pm j}$ constitute a pair of Kramers degenerate doublets with energies (34). For nonzero ε, the splitting between the doublets never vanishes. If we consider $N \gg 1 \geq |\alpha|$, i.e., being reasonably close to the classical limit for the slow subsystem, the energies of these doublets are nearly opposite, and consequently, the $\pm$ signs in (34) correspond to the "bulk" states belonging permanently to the upper and lower bands[12], see fig. 6.

It remains to find out what happens to the edge states. As before in sec. 3.1.2, they are readily constructed as single states $\psi_{\pm(N+S)}$ which are not affected by the nondiagonal terms in (32). Engaging only the diagonal part of the first (principal) term of (31), we obtain

$$\hat{H}^1_\alpha \psi_\pm = \frac{\alpha}{NS} N_1 S_1 \psi_\pm = \frac{\alpha}{NS}(\pm N)\left(\pm\tfrac{1}{2}\right)\psi_\pm = \alpha\,\psi_\pm\ .$$

So the two "edge" states form an exceptional Kramers doublet with energy α which is redistributed between the two bands top down as α decreases from 1 to -1, see fig. 6.

4.2. **Linearization of Kramers-degenerate systems.** Linearization near the sole degeneracy point of the original spin-obit system in sec. 3 lead to the Dirac oscillator. Applying the same approach to the $\mathcal{T}$-invariant Kramers-degenerate system with Hamiltonian (31–32), requires *two independent linearizations* at poles $N_1/N = \pm 1$ of the slow space $\mathbb{S}^2_N$. These linearizations differ in the definition of local symplectic coordinates (q, p) which are summarized in (8).

Replacing N_1 and $N_\pm$ in (32) according to (8) gives the spinor forms of the Hamiltonian (32) linearized near each pole

$$\hat{H}^1_\alpha\big|_{N_1=+N} = \alpha\begin{pmatrix}-1 & 0\\ 0 & 1\end{pmatrix} + \frac{2\alpha}{\sqrt{2N}}\begin{pmatrix}0 & a^-\\ a^+ & 0\end{pmatrix} - \frac{2\varepsilon\,\mathrm{i}}{\sqrt{2N}}\begin{pmatrix}0 & a^-\\ -a^+ & 0\end{pmatrix}, \tag{36a}$$

$$\hat{H}^1_\alpha\big|_{N_1=-N} = \alpha\begin{pmatrix}1 & 0\\ 0 & -1\end{pmatrix} + \frac{2\alpha\,\mathrm{i}}{\sqrt{2N}}\begin{pmatrix}0 & a^+\\ -a^- & 0\end{pmatrix} + \frac{2\varepsilon}{\sqrt{2N}}\begin{pmatrix}0 & a^+\\ a^- & 0\end{pmatrix}. \tag{36b}$$

Their respective operator forms are obtained from (30a), (31), and (8)

$$\hat{H}^1_\alpha\big|_{N_1=+N} = \ \alpha\,\frac{S_1}{S} + \alpha\,\frac{a^-S_- + a^+S_+}{\sqrt{2NS}} - \mathrm{i}\varepsilon\,\frac{a^-S_- - a^+S_+}{\sqrt{2NS}}\ , \tag{37a}$$

$$\hat{H}^1_\alpha\big|_{N_1=-N} = -\alpha\,\frac{S_1}{S} + \mathrm{i}\alpha\,\frac{a^+S_- - a^-S_+}{\sqrt{2NS}} + \varepsilon\,\frac{a^+S_- + a^-S_+}{\sqrt{2NS}}\ . \tag{37b}$$

[12] It can be thus observed that bulk states have a solid classical interpretation while the existence of the edge states remains an essentially quantum phenomenon. This is known as bulk-edge correspondence in topological insulators [9].

Similarly to (28), Hamiltonians (36a) and (36b) have first integrals $\hat{n} - \hat{S}_1$ and $\hat{n} + \hat{S}_1$, respectively, with spinor forms

$$\hat{n} \pm \hat{S}_1 = \begin{pmatrix} n \mp \frac{1}{2} & 0 \\ 0 & n \pm \frac{1}{2} \end{pmatrix}. \tag{38}$$

This follows from direct computation of commutators of (38) and (36). At the same time, it is instructive to see integrals (38) as linearizations of $\hat{J}_1$ in (25). To this end recall that in the Holstein–Primakoff approximation [20] near each pole (8) of the slow phase space $\mathbb{S}^2_N$, the angular momentum N_1 equals[13] $\mp N \pm n$, where n is the number of quanta in the local harmonic oscillations about the poles. Consequently, the spinor form (25) of J_1 becomes

$$\hat{J}_1\big|_{N_1=\pm N} = \begin{pmatrix} \pm N \mp n - \frac{1}{2} & 0 \\ 0 & \pm N \mp n + \frac{1}{2} \end{pmatrix} = \pm \hat{1} N \mp \hat{n} + \hat{S}_1$$

which is, to a sign and a constant scalar term $\hat{1}N$, equivalent to (38). We also recognize the first integral of the Dirac oscillator (sec. 2.2).

We further notice that systems with Hamiltonians (36) and respective first integrals (38) are related by time-reversal symmetry $\mathcal{T}$ in (6). While this operation maps the polar regions of $\mathbb{S}^2_N$ into each other, it interchanges the symplectic coordinates (q, p) in these regions as well as changes their sign. We have

$$\mathcal{T} : (\boldsymbol{S}, q, p) \mapsto -(\boldsymbol{S}, p, q) \quad \text{and} \quad \mathcal{T} : a^{\pm} \to \pm \mathrm{i} a^{\mp}.$$

It can be seen that Hamiltonians (37) are related by this operation and that so are the respective semi-quantum spinor matrices (36), cf. footnote 5. As a result, Hamiltonians (36) are *isospectral*. Furthermore, to a reparameterization, their spectra are equivalent to that of the Dirac oscillator in sec. 2.2. The eigenstates of either (36a) or (36b) have nondegenerate eigenvalues, with a single "edge" state of energy α and the "bulk" states forming two bands with a pseudo-symmetric spectrum.

We compute the spectrum. Since both (11) and (36b) commute with $\hat{n} + \hat{S}_1$, we can work on the Hilbert subspaces $\mathcal{H}_k$ with $k - \frac{1}{2} = n \in \mathbb{Z}_{>0}$ of functions ψ_k already defined in sec. 2.2. On these subspaces, we find the corresponding bulk state eigenvalues

$$\lambda_n = \pm \sqrt{\frac{2n}{N}(\varepsilon^2 + \alpha^2) + \alpha^2} \tag{39}$$

while the single edge state ψ_0 of (36b) has energy α, see fig. 7. The bands are separated at least by $\pm\varepsilon\sqrt{2/N}$. Scaling these energies by $\sqrt{2(\varepsilon^2 + \alpha^2)/N} > 0$ gives the spectrum of the Dirac oscillator in fig. 1 with

$$\mu = -\alpha \sqrt{\frac{N}{2\,(\varepsilon^2 + \alpha^2)}}\,.$$

[13] Indeed, Taylor expanding

$$N_1 = \pm\sqrt{\|\boldsymbol{N}\|^2 - N_2^2 - N_3^2} \approx \pm\|\boldsymbol{N}\|\left(1 - \frac{N_2^2 + N_3^2}{2\|\boldsymbol{N}\|^2}\right) = \pm\|\boldsymbol{N}\| \mp \frac{q^2 + p^2}{2}$$

and using the semiclassical value $\|\boldsymbol{N}\| = N + \frac{1}{2}$, we obtain

$$N_1/N \approx \pm 1 \mp I = \pm 1 \mp n$$

with oscillator action $I = \frac{1}{2}(q^2 + p^2)$ acting as $\hat{I}|n\rangle = (n + \frac{1}{2})|n\rangle$.

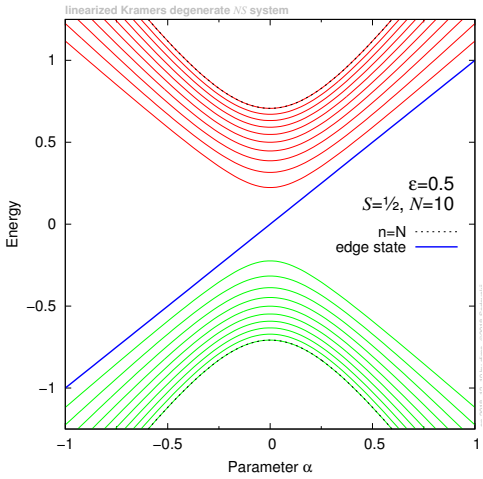

FIGURE 7. Spectrum of the system with Hamiltonian (36b) obtained as linearization of $\mathcal{T}$-reversal $\boldsymbol{NS}$, $S = \frac{1}{2}$ Hamiltonian (32) for coupling parameter $\alpha \in [-1, 1]$. Compare to fig. 1 and 6. The bulk state energies (red and green lines) are given by (39).

In order to finalize the description of the spectrum, we turn to the spinor Hamiltonian (36a) (linearization at $N_1/N = 1$). This operator commutes with $\hat{n} - \hat{S}_1$. We should, therefore, work on the Hilbert subspaces of eigenfunctions of $\hat{n} - \hat{S}_1$

$$\mathcal{H}^*_k \ni \psi^*_k = \sum_\sigma c_{\sigma,k} |\tfrac{1}{2}, \sigma\rangle |k + \sigma\rangle, \quad \text{where } k + \tfrac{1}{2} = n \in \mathbb{Z}_{>0},$$

with eigenvalue k. These subspaces contain the bulk states. The action of (36a) on ψ^*_n has the bulk eigenvalues identical to (39). The sole edge function

$$\psi^*_{-\frac{1}{2}} = |\tfrac{1}{2}, \tfrac{1}{2}\rangle |0\rangle$$

is the eigenfunction of $\hat{n} - \hat{S}_1$ with eigenvalue $-\frac{1}{2}$. The energy of this edge state equals α. We conclude that the entire spectrum of the original system with Hamiltonian (29) is reproduced as a sum of two identical spectra (39). Each of these spectra corresponds to a Dirac oscillator, a system without $\mathcal{T}$-invariance. Their sum reproduces Kramers degeneracy of the $\mathcal{T}$-invariant system (footnote 5).

4.3. **Combining Dirac oscillators and Chern indices.** Our results in sec. 3.2 suggest that the redistribution phenomenon in the $\mathcal{T}$-invariant system can be analyzed entirely by exploiting what we know already for simpler systems in sec. 2.1, 2.2, and 3. The eigenstate bundles $\Lambda_{1,2}$ over $\mathbb{S}^2_N$ have Chern indices $c_1 = \pm 1$. More specifically, denoting these bundles as $\Lambda_\pm$ for positive/negative semi-quantum energies (33) respectively, we find (Appendix A.6 and A.7) $c_1 = \mp 1$ for $\alpha > 0$ and ± 1 for $\alpha < 0$, cf. fig. 5. The *index change* $|\delta c_1|$ of 2 corresponds to the *two* edge states (forming one Kramers doublet) exchanged at $\alpha = 0$. Alternatively, within the standard geometric phase framework, the eigenbundles are constructed *locally*, near each degeneracy point, after the total degeneracy at $\alpha = 0$ is removed by the ε-term. The computations are equivalent to those for the original system with Hamiltonian (22) near its sole degeneracy with $N_1 = -N$ and $\gamma = \frac{1}{2}$ and for the Dirac oscillator in sec. 2.2. Two linearizations $\lambda(\alpha, N_2, N_3)|_{N_1 = \pm N}$ are required,

leading to the analysis of the eigenbundles $\Delta_{1,2}\big|_{N_1=\pm N}$. In this way, choosing an appropriate sign convention, we obtain $c_1 = 1$ for Δ_1 defined near either of the poles, giving the total of $+2$, while for Δ_2, the indices have opposite signs totalling up to -2, see Appendix A.7. This sum of indices computed locally near each pole corresponds to the total number of gained/lost levels by the corresponding energy band.

5. **Quadratic spin-orbit coupling.** As we explain in sec. 2.3, the $\mathcal{T}$-invariant system in sec. 4 cannot provide a dynamical analogy of the spin-quadrupole systems in [31, 5] because the spin-orbit Hamiltonian (31) has no $\mathcal{T}_S$ symmetry. At the same time, for lack of a better idea and because it seems quite a reasonable thing to begin with when moving into unknown territory, we like to recycle the approach of sec. 4. Recall that in order to construct a two-band system with elementary $\mathcal{T}$-equivariant energy level redistribution, we retained the spherically symmetric spin-orbit term (2) and we used its coefficient α as the principal (sole) parameter of the system. In order to lift the complete collapse of the bands at $\alpha = 0$, we added an ε-term (30b) with specific properties making the sign and the concrete value of ε unimportant as long as $\varepsilon \neq 0$.

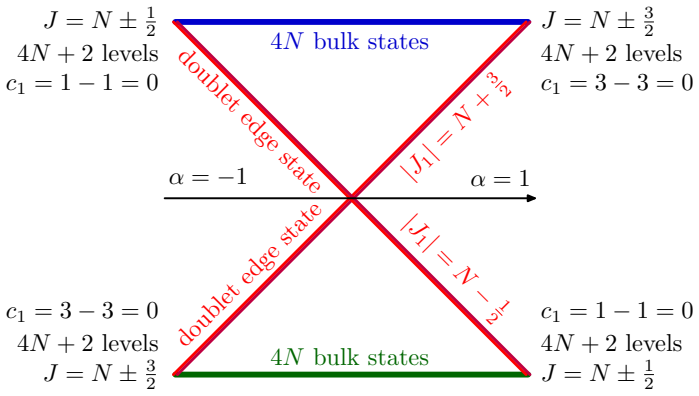

FIGURE 8. Correlation diagram for the quadratic dynamical spin-quadrupole system in sec. 2.3.2 with the conjectured $\mathcal{T}_S \times \mathcal{T}_N$-equivariant deformation in sec. 5, spin $S = \frac{3}{2}$, and $N \gg S$ as function of formal control parameter α of the isotropic quadrupolar coupling term (18). The values ± 1 of α correspond to the coupled system with Hamiltonian (18) times ± 1. Bold solid lines represent the energies of the bulk states (blue and green) and of the two Kramers doublet edge states (red) exchanged in opposite directions. Unlike the indices c_1 in fig. 2 and 4 which can be computed in the standard way for the $\Lambda_{1,2}$ bundles on $\mathbb{S}^2_N$ (see sec. 1.2 and 2.1), the values of c_1 in this diagram are conjectured so that they agree with the number of states in each band. See text for more detail.

The isotropic Hamiltonian (18) introduced in sec. 2.3.2 seems to be a most natural choice for the quadratic α-term. However, before we attempt constructing the $\mathcal{T}_S$-invariant and, possibly, axially symmetric quadratic ε-term (sec. 5.1), we should pay attention to one important difference between (18) and plain linear spin-orbit

Hamiltonian (2). As we show in sec. 2.3.3, the spectrum of the spin-$\frac{3}{2}$ system with Hamiltonian (18) and the spectrum of the spin-$\frac{1}{2}$ system with plain spin-orbit Hamiltonian (2b) have both two bands. However, while the latter system has bands with different number of states, the bands of the former system have equal number of levels (proposition 1).

More specifically, the bands of the spin-$\frac{3}{2}$ system with Hamiltonian (18) can be seen as two "super-bands", each having two complete multiplets of $2J+1$ states with a fixed value of $J = N-S, \dots, N+S$ as two "sub-bands". These "sub-bands" appear naturally for large $|\alpha|$ after adding small perturbation term $\boldsymbol{S}\cdot\boldsymbol{N}$ preserving the time reversal symmetry (6) and the SO(3) isotropy but breaking the $\mathcal{T}_S$ symmetry. Sub-bands have different J and differ in the number of levels, but each super-band has the same total number of levels. Nevertheless, the super-bands are qualitatively different because the values of J are unique. This makes the limits of $\alpha = -1$ and $\alpha = +1$ qualitatively different and when α changes sign, a number of states must be redistributed to rebuild the two super-bands. However, since the total number of states remains unchanged, the redistribution should go *both* ways. From the detailed classification of states in each band given in proposition 1, we can conjecture that the two Kramers doublets with $|J_1| = N+S$ and $|J_1| = N+S-2$ have to be exchanged. Assuming that both $\mathcal{T}_S$ and $\mathcal{T}_N$ symmetries (sec. 2.3.1) are preserved by the ε-deformation, i.e., that the $\mathcal{T}$ symmetry is also present and Kramers doublets remain intact, the entire redistribution is given by the correlation diagram in fig. 8.

In this diagram, the hypothetical values of the super-bands indices c_1 and their decomposition into a sum of two sub-band indices are deduced from the total number of states in each super-band and sub-band. Compared to the previous sections, the actual calculation of these indices is now hampered by the degeneracy of the semi-quantum eigenvalues. The four eigenstates of the $\mathcal{T}_S$-symmetric spin-$\frac{3}{2}$ semi-quantum system form two Kramers doublets which correspond to the super-bands. The Λ-bundle for each super-band is, therefore, formed by two semi-quantum eigenstates with degenerate eigenvalue $\lambda : \mathbb{S}^2_N \to \mathbb{R}$. Assuming that this Λ-bundle can be decomposed continuously over $\mathbb{S}^2_N$ into two respective sub-bundles, these indices can be computed. The linearization in sec. 5.2 may suggest that such decomposition is indeed possible. At the same time, the difference of the indices, or delta-Chern $\delta c_1 = 0$, can be confirmed as previously (sec. 2.2) using the linearization in sec. 5.2. The calculation of Chern indices for superbands, i.e., for the rank-2 bundles, is discussed in appendix A.8.

5.1. **The family of quadrupolar spin-orbit Hamiltonians.** Using tensors $\boldsymbol{T}^2$ introduced in sec. 2.3.2 and incorporating spherically symmetric α-term (18), the closest degree-2 analog of (31) can be written as

$$\hat{H}_{\alpha_0} = \alpha_0\sqrt{5}\left[\boldsymbol{T}^2(\hat{\boldsymbol{S}})\times\boldsymbol{T}^2(\hat{\boldsymbol{N}})\right]^0 + \mathrm{i}\varepsilon\sqrt{5}\,\frac{\sqrt{2}}{\sqrt{3}}\left[\boldsymbol{T}^2(\hat{\boldsymbol{S}})\times\boldsymbol{T}^2(\hat{\boldsymbol{N}})\right]^1_0\,, \tag{40a}$$

$$= \alpha_0\left(\left(\hat{\boldsymbol{S}}\cdot\hat{\boldsymbol{N}}\right)^2 - \frac{1}{3}\hat{\boldsymbol{S}}^2\hat{\boldsymbol{N}}^2\right) + \varepsilon\,\frac{1}{\sqrt{3}}\left[\hat{\boldsymbol{S}}\cdot\hat{\boldsymbol{N}},\,\left(\hat{\boldsymbol{S}}\wedge\hat{\boldsymbol{N}}\right)\cdot\boldsymbol{e}_1\right]_+\,. \tag{40b}$$

This Hamiltonian is axially symmetric and is invariant under both $\mathcal{T}_S$ and $\mathcal{T}_N$ reversal symmetries in sec. 2.3.1. Similarly to its predecessor (30b), the axially-symmetric ε-term in (40) incorporates the exterior product of $\boldsymbol{S}$ and $\boldsymbol{N}$ (of rank

1). In the basis (16), this term contributes solely to the off-diagonal block

$$\hat{\mathsf{M}} = \frac{1}{2}\begin{pmatrix} (\alpha_0\sqrt{3}+\mathrm{i}\varepsilon)[N_1,N_+]_+ & (\alpha_0\sqrt{3}-2\,\mathrm{i}\varepsilon)N_-^2 \\ (\alpha_0\sqrt{3}+2\,\mathrm{i}\varepsilon)N_+^2 & -(\alpha_0\sqrt{3}-\mathrm{i}\varepsilon)[N_1,N_-]_+ \end{pmatrix}. \tag{41}$$

of the quaternion-form matrix (17) of (40).

5.1.1. *Semi-quantum energies.* The system has, as expected, a pair of pseudo-symmetric semi-quantum eigenvalues

$$\lambda_\pm(\alpha_0,\boldsymbol{N}) = \pm N\sqrt{(\alpha_0^2+\varepsilon^2)N^2-\varepsilon^2N_1^2} = \pm N^2\sqrt{\alpha_0^2+\varepsilon^2\sin^2\theta}\,, \tag{42}$$

the same as (33) but with multiplicity 2. Figuratively, multiplicity doubles all features of the semi-quantum system in sec. 4.

Thus, critical semiquantum energies in fig. 9 and fig. 6 are the same. In particular, for all $\alpha_0 \neq 0$, the eigenvalue $\lambda_+(\alpha_0,\boldsymbol{N})$ has a double minimum at the poles, and a degenerated maximal circle on the equator. Degeneracy occurs only at energy 0 and only when $\alpha_0 = 0$ and only as conical intersections at the poles $\{N_1 = \pm N\}$.

5.1.2. *Quantum spectrum.* The quantum spectrum of (40) with nonzero ε requires numerical diagonalization (typically of 4×4 matrices). As can be clearly seen in fig. 9, for large $|\alpha_0| \gg \varepsilon > 0$, this spectrum tends to the SO(3) isotropic limit which is analyzed in detail in sec. 2.3.3. Specifically, we can see how the states in this limit regroup into subbands with given total angular momentum J.

It is instructive to consider the spectrum for $\alpha_0 = 0$, i.e., the eigenstates of the ε-term of (40). These eigenstates, labelled by the absolute value $|J_1|$ of momentum J_1, are represented in fig. 10 in the form of an energy-momentum diagram. We notice that, similarly to that of (30b), the spectrum of the ε-term in (40) is pseudo-symmetric (the eigenvalues come either in $\pm$ pairs or equal 0), and is non-degenerate on each Hilbert space $\mathcal{H}_{J_1}$ spanned by eigenfunctions of $\hat{J}_1$ with given fixed eigenvalue J_1. This follows from the fact that both these ε-terms have imaginary skew-symmetric matrices which are not block-diagonal unless $\dim\mathcal{H}_{J_1}$ is odd, in which case there is one zero eigenvalue. As fig. 10 illustrates, and in accordance with proposition 1, the two edge state doublets in the spin-$\frac{3}{2}$ spectrum of the ε-term of (40) have unambiguous superband destination in the isotrpic limits with $|\alpha_0| \gg \varepsilon$. The destination is predefined by the conserved value of $|J_1|$. For example, the doublet with the maximal $|J_1| = N+\frac{3}{2}$ joins necessarily the multiplet with the maximal $J = N+\frac{3}{2}$ of the $J = N\pm\frac{3}{2}$ superband.

5.2. **Linearization at the degeneracy points.** The $\mathrm{SO}(2)\wedge(\mathcal{T}_S\times\mathcal{T}_N)$-invariant Hamiltonian (40) in sec. 5.1 can be linearized straightforwardly tracing the outline in the beginning of sec. 4.2. Linearizing at both poles of the classical slow phase space $\mathbb{S}^2$ and using (8) produce two *isospectral* systems with $\mathcal{T}_S$-invariant (but *not* $\mathcal{T}$-invariant) Hamiltonians

$$\hat{H}_{\alpha_0}\big|_{N_1=\pm N} = N^2\,\hat{\boldsymbol{S}}\tilde{\mathsf{Q}}\hat{\boldsymbol{S}} \quad \text{with } \tilde{\mathsf{Q}} = N^{-2}\mathsf{Q}\big|_{N_1=\pm N}\,. \tag{43}$$

The elements (see footnote 9) of the linearized matrices $\tilde{\mathsf{Q}}$ in (43) are given by

$$\tilde{Q}_{xx} = \tilde{Q}_{yy} = -\frac{1}{3}\,\alpha_0, \qquad \tilde{Q}_{zz} = \frac{2}{3}\,\alpha_0, \qquad \tilde{Q}_{xy} = 0, \qquad \text{for } N_1 = \pm N$$

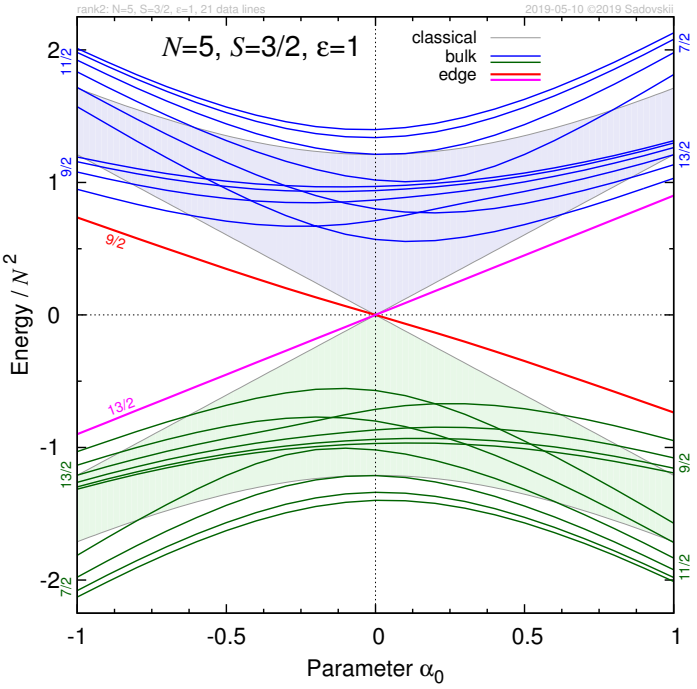

FIGURE 9. Spectrum of the Kramers degenerate $\mathcal{T}_N \times \mathcal{T}_S$-invariant axially symmetric system of coupled angular momenta $\boldsymbol{S}$ (fast) and $\boldsymbol{N}$ (slow) of conserved lengths $S = \frac{3}{2}$ and $N = 5$ with Hamiltonian (40) as function of the "quaternionic" spin-orbit coupling parameter α_0. Solid color lines represent quantum Kramers doublet states. Specifically, the bulk state energies are depicted in blue and green, while red and purple correspond to the two edge state doublets. For the end values ± 1 of α_0, the levels within each band reassemble visibly into multiplets with conserved length J of the total angular momentum $\boldsymbol{N} + \boldsymbol{S}$ and the respective values of J are marked along the left and right vertical axes, cf. sec. 2.3.3. The edge states are distinguished by the conserved value of J_1 displayed near the $\alpha_0 = -1$ end of the plot. The boundaries of the lightly shaded semi-quantum energy domains (gray lines) are given by (42) where N_1 takes one of the critical values $\{N, 0\}$ and with N replaced by $N_{\text{classical}} = N + \frac{1}{2}$.

and

$$\tilde{Q}_{xz} = +\frac{1}{\sqrt{N}}\left(\alpha_0\, q - \frac{\varepsilon}{\sqrt{3}}\, p\right), \quad \tilde{Q}_{yz} = +\frac{1}{\sqrt{N}}\left(\alpha_0\, p + \frac{\varepsilon}{\sqrt{3}}\, q\right), \quad \text{for } N_1 = +N,$$
$$\tilde{Q}_{xz} = -\frac{1}{\sqrt{N}}\left(\alpha_0\, p - \frac{\varepsilon}{\sqrt{3}}\, q\right), \quad \tilde{Q}_{yz} = -\frac{1}{\sqrt{N}}\left(\alpha_0\, q + \frac{\varepsilon}{\sqrt{3}}\, p\right), \quad \text{for } N_1 = -N.$$

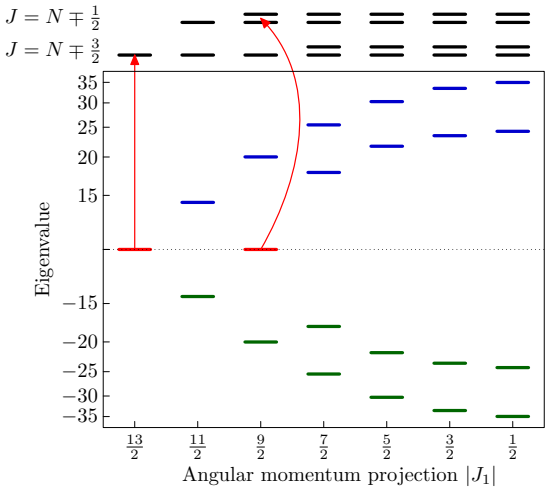

FIGURE 10. Joint spectrum of the ε-term of the quadratic spin-orbit Hamiltonian (40) and $\hat{J}_1$. The values of spin $S = \frac{3}{2}$ and slow angular momentum $N = 5$ correspond to fig. 9. Bold solid bars represent the bulk states (blue and green) and two Kramers doublet edge states (red). Above the energy-momentum diagram, we show the composition of the two multiplets in each superband of the spectrum of the isotropic term in sec. 2.3.3. Red arrows indicate which of the subbands takes in the particular edge states, see proposition 1.

In the spinor basis (16), Hamiltonian (43) becomes a matrix operator with quaternionic matrix of the form (17). It has diagonal parameter

$$g\big|_{N_1=\pm N} = -\alpha_0\, N^2 \tag{44a}$$

and the off-diagonal block

$$\hat{\mathsf{M}}\big|_{N_1=+N} = +\begin{pmatrix} \beta\, a^- & 0 \\ 0 & -\bar{\beta}\, a^+ \end{pmatrix}, \tag{44b}$$

$$\hat{\mathsf{M}}\big|_{N_1=-N} = -\mathrm{i}\begin{pmatrix} \beta\, a^+ & 0 \\ 0 & \bar{\beta}\, a^- \end{pmatrix}, \qquad \text{with } \beta = (\alpha_0\sqrt{3} + \mathrm{i}\varepsilon)N\sqrt{2\,N}\ . \tag{44c}$$

In the basis $\{|\frac{3}{2}, -\frac{1}{2}\rangle, |\frac{3}{2}, -\frac{3}{2}\rangle\} \oplus \{|\frac{3}{2}, \frac{3}{2}\rangle, |\frac{3}{2}, \frac{1}{2}\rangle\}$, this matrix becomes block-diagonal

$$\operatorname{diag}\left(\hat{H}, -\hat{H}\right) \text{ with } \hat{H} = \begin{pmatrix} g & h \\ h^\dagger & -g \end{pmatrix} \tag{45a}$$

where

$$h = \beta\, a^- \text{ for } N_1 = N \quad \text{and} \quad h = -\mathrm{i}\,\beta\, a^+ \text{ for } N_1 = -N. \tag{45b}$$

To a sign and a scalar factor, $\hat{H}$ is isospectral to one of Hamiltonians (36). They all are, essentially, Dirac oscillators (11). The sign is important as it defines the transfer direction of the sole edge state in each block (see fig. 7). Linearizations for $N_1 = +N$ or $-N$ are isospectral, $\mathcal{T}_N$ invariance obliging. Superposition of the spectra of the $\pm\hat{H}$ blocks for either linearization gives *two* edge states transferred in *opposite* directions.

5.3. **Redistribution, Chern indices, and the number of states.** Linearization in sec. 5.2 elucidates the point that we have already made when discussing semiquantum energies (42) : our system is a double cover of the one in sec. 4.1 with the two copies having opposite redistribution directions. Due to the multiplicity of (42), the semi-quantum system has *four* degeneracy points, each point corresponding to one of the four quantum edge states exchanged as suggested by the correlation diagram in fig. 8 and confirmed by the concrete computation represented in fig. 9. The four quantum edge states are grouped into two Kramers doublets, while the respective four degeneracy points form two pairs with the points in each pair related by the $\mathcal{T}_N$ symmetry operation. Comparing to the redistribution phenomenon in fig. 5 of sec. 4, we have now twice as many degeneracy points and edge state doublets. For each doublet (and respective pair of $\mathcal{T}_N$-equivalent points at the poles), the phenomenon is the same as in sec. 4.

In general, on the entire interval of the tuning control parameter α_0, the four individual semiquantum eigenvalues (42) form two bundles $\Lambda^{\pm}$ of rank two, their superscripts $\pm$ replicating the sign of (42) and so referring to the upper and lower superbands. There is no further natural decomposition of the $\pm$ eigenspaces into a direct sum of one-dimensional subspaces. In fact, as we can see in fig. 9, there is no continuous uniform way to represent the bulk spectrum of (40) as a sum of Dirac oscillator spectra similarly to the way it was possible previously in sec. 3 and 4. On the other hand, the linearization in sec. 5.2 and the SO(3)-isotropic limit in sec. 2.3.2 and 2.3.3 provide certain grounds for the conjecture that $\Lambda^{\pm}$ at large $|\alpha_0|$ split into bundles $\Lambda^{\pm}_{1,2}$ where the subscripts $(1,2)$ account for multiplicity 2 of (42). Then in the limit of large $|\alpha_0|$, as indicated in fig. 8, we should find $c_1 = \pm 3$ for one pair of $\Lambda_{1,2}$ and $c_1 \pm 1$ for the other. These indices correspond to the number of states in the multiplets of the isotropic system, see proposition 1. In both cases, the sum of Chern indices gives index 0 for the rank-2 bundles $\Lambda^{\pm}$. Continuing from the large $|\alpha_0|$ limits towards the degeneracy point $\alpha_0 = 0$, we can assume that c_1 indices of $\Lambda^{\pm}$ remain zero. For the quantum system, such combined zero index means that the total number of states in each superband equals $2(2N+1)$, including $2N$ bulk state doublets plus one edge state doublet, see fig. 8. This number is given by twice the phase space volume of $\mathbb{S}^2_N$ without any corrections.

On the other hand, within the geometric phase framework, we should consider four local bundles $\Delta^{\pm}_{1,2}$ over spheres $\mathbb{S}^2$ enclosing one of the two degeneracies. This can be combined with one of the linearizations in sec. 5.2 which have formal control parameter α_0 and dynamical parameters (q,p). For each linearization, we study the bundles Δ over the base $\mathbb{S}^2 \subset \mathbb{R}_{\alpha_0,q,p}$ enclosing the origin. Like in sec. 4.2, Kramers degeneracy ensures that the analysis for linearization at the poles $\{N_1 = N\}$ and $\{N_1 = -N\}$ gives the same result. For example, if $\Delta\big|_{N_1=N}$ has index $c_1 = 1$, then so does $\Delta\big|_{N_1=-N}$. Block-diagonal form (45) means that for either linearization, we can construct unambiguously four bundles $\Delta^{\pm}_1$ and $\Delta^{\pm}_2$, where $(1,2)$ label Dirac oscillator factor-blocks in (45) and $\pm$ refer to the upper and lower superbands. Since the oscillator blocks are of opposite signs, $\Delta^{\pm}_1$ and $\Delta^{\pm}_2$ have indices $c_1 = \mp 1$ and $c_1 = \pm 1$, respectively. So, for example, for Δ^{+}_1 and Δ^{+}_2 with indices $c_1 = -1$ and $c_1 = +1$ this means that one subband of the upper superband looses a state (to the lower superband) while the other subband of the same superband gains a state (from the lower superband). Adding up for two linearizations, we reconstruct lost/gained Kramers doublets. At the same time, the sum of indices for either $\Delta^{+}_{1,2}$

or $\Delta^{-}_{1,2}$ gives zero, reflecting that the number of states in the superbands remains unchanged.

6. **Discussion.** The simple Hamiltonian (1) has been widely recognized as relevant in many different physical problems [43]. The geometric phase phenomenon in the parametric family of model systems with this Hamiltonian is directly related to the fundamental mathematical construction of vector bundles, realized as eigenstate bundles over the parameter space, and to the naturally defined connections on these bundles and topological invariants [38]. The parallel discovery of the quantum Hall effect [40, 26], topological insulators, and more generally, topological phase transitions and topological phases of matter [39] have arisen considerable interest in topological effects mainly in solid state and high-energy physics. On the other hand, despite being suggested very early, the same year as the paper by Haldane [18] on the Hall effect, the dynamical modification of the geometrical phase setup [36] in finite particle systems with compact phase spaces and its relation to the separation of slow and fast variables and associated rearrangement of energy bands met with little enthusiasm in molecular and atomic physics. One possible reason may be that there are still many important discrete quantum states of these systems that can be studied individually, repeatedly, and with ever increasing accuracy, while large groups of levels, such as polyads, multiplets, shells, and generally—bands require higher excitations, special conditions, and are difficult to reach experimentally, to interpret, and to investigate theoretically. Yet energy bands and their rearrangements are common features of excited molecular systems and their thorough investigation is impending.

Our work reviewed and summarized the universal properties of slow-fast parametric semi-quantum systems with one slow degree of freedom and paws the way for the study of systems with two slow degrees of freedom (four dynamical parameters), specifically the 4-level quaternionic semiquantum systems and their full quantum analogues, and more concretely, the model quadratic spin systems with time-reversal symmetry and spin $\frac{3}{2}$, which are direct dynamical analogues of [31, 6]. These systems have a slow phase space P of dimension four supplemented by one formal control parameter. The local semi-quantum eigenstate bundles Δ and the semi-quantum eigenstate bundles Λ over P are now characterized by the second index c_2 (cf. [13, 14]). This brings up the fundamental question of how the value of c_2 and its change are reflected by the numbers of quantum states in the corresponding energy bands and by the redistribution phenomenon, respectively. This question remains yet to be fully addressed. Several compact and non-compact possibilities for P can be envisaged and their analysis promises to be of great interest and importance to mathematical theory and physical applications.

Appendix A. **Chern number calculations.** This appendix presents explicit calculations of Chern numbers for eigenstate bundles of several semi-quantum systems analyzed in the main body of the article. The relation between Berry setup [10] and topological Chern numbers was immediately recognized by Simon [38] and concrete calculations of Chern numbers for the model Hamiltonian (1) were described about 30 years ago by Avron and co-authors [6] along with more difficult calculations for the quadratic spin Hamiltonian (cf. sec. 2.3). We reproduce these calculations for concrete Hamiltonians following the outline in [21].

A.1. **Chern numbers for a spin-orbital coupling system.** Let us consider the semi-quantum angular momentum coupling Hamiltonian (2a) for $S = \frac{1}{2}$, which is expressed in the basis $\{|\frac{1}{2}, \frac{1}{2}\rangle, |\frac{1}{2}. -\frac{1}{2}\rangle\}$ as

$$H = \frac{1}{2}\begin{pmatrix} N_1 & N_- \\ N_+ & -N_1 \end{pmatrix}, \quad N_\pm = N_2 \pm \mathrm{i}N_3, \tag{46}$$

cf. (4) and recall that in the semi-quantum setting, we view the "slow" angular momentum operator $\hat{\boldsymbol{N}}$ as a classical vector variable $\boldsymbol{N}$. This brings us within the geometric phase setup [38]. The eigenvalues of the semi-quantum Hamiltonian

$$\lambda_\pm(\boldsymbol{N}) = \pm\frac{1}{2}N, \quad N = \|\boldsymbol{N}\| \tag{47}$$

are obtained straightforwardly. The eigenvector associated with $\lambda_+(\boldsymbol{N})$ can be expressed in two ways

$$|u^+_{\mathrm{up}}\rangle = \frac{1}{N^+_{\mathrm{up}}}\begin{pmatrix} N_2 - iN_3 \\ N - N_1 \end{pmatrix}, \quad N^+_{\mathrm{up}} = \sqrt{2N(N - N_1)}\,, \quad \text{and} \tag{48a}$$

$$|u^+_{\mathrm{down}}\rangle = \frac{1}{N^+_{\mathrm{down}}}\begin{pmatrix} N + N_1 \\ N_2 + iN_3 \end{pmatrix}, \quad N^+_{\mathrm{down}} = \sqrt{2N(N + N_1)}\,. \tag{48b}$$

It should be pointed out that $|u^+_{\mathrm{up}}\rangle$ and $|u^+_{\mathrm{down}}\rangle$ cannot be defined at the north (N) and the south (S) poles of the two-sphere $\mathbb{S}^2_N$ of radius N, respectively. In other words, their respective domains are

$$U^+_{\mathrm{up}} = \mathbb{S}^2_N \setminus \mathrm{N} \quad \text{and} \quad U^+_{\mathrm{down}} = \mathbb{S}^2_N \setminus \mathrm{S}\,. \tag{49}$$

We call the points where the eigenvectors cannot be defined *exceptional*. On the intersection $U^+_{\mathrm{up}} \cap U^+_{\mathrm{down}}$, the eigenvectors $|u^+_{\mathrm{up}}\rangle$ and $|u^+_{\mathrm{down}}\rangle$ are related by

$$|u^+_{\mathrm{up}}\rangle = \eta\,|u^+_{\mathrm{down}}\rangle \quad \text{with } \eta = \frac{N_2 - \mathrm{i}N_3}{\sqrt{N_2^2 + N_3^2}} = \exp(-\mathrm{i}\phi)\,. \tag{50}$$

This relation and (48) determine the eigenvector bundle Λ_+ over $\mathbb{S}^2_N$ associated with eigenvalue $\lambda_+(\boldsymbol{N})$. The local connection forms are defined, respectively, as

$$A^+_{\mathrm{up/down}} = \langle u^+_{\mathrm{up}}|\mathrm{d}|u^+_{\mathrm{up/down}}\rangle, \tag{51}$$

and are related on $U_{\mathrm{up}} \cap U_{\mathrm{down}}$ by

$$A^+_{\mathrm{up}} = A^+_{\mathrm{down}} + \eta^{-1}\mathrm{d}\eta. \tag{52}$$

The local curvature forms are defined, respectively, as

$$F^+_{\mathrm{up/down}} = \mathrm{d}A^+_{\mathrm{up/down}}. \tag{53}$$

Since $F^+ := F^+_{\mathrm{up}} = F^+_{\mathrm{down}}$ on $U^+_{\mathrm{up}} \cap U^+_{\mathrm{down}}$, the curvature form F^+ is defined globally on $\mathbb{S}^2_N$.

In order to evaluate the first Chern number c_1 of Λ_+, we integrate the curvature form F^+ over $\mathbb{S}^2_N$ with spherical coordinates (θ, ϕ). Let $\mathbb{S}^2_{N+}$, $\mathbb{S}^2_{N-}$, and $\mathbb{S}^1_N$ denote the northern and southern hemispheres, and of the equator of $\mathbb{S}^2_N$. Then, the integral of F^+ over $\mathbb{S}^2_N$ is calculated using the Stokes theorem, (50), and (52)

$$\begin{aligned}\int_{\mathbb{S}^2_N} F^+ &= \int_{\mathbb{S}^2_{N+}} F^+_{\mathrm{down}} + \int_{\mathbb{S}^2_{N-}} F^+_{\mathrm{up}} = \int_{\mathbb{S}^1_N} (A^+_{\mathrm{down}} - A^+_{\mathrm{up}}) \\ &= -\int_{\mathbb{S}^1_N} \eta^{-1} d\eta = \mathrm{i}\int_0^{2\pi} \mathrm{d}\phi = 2\pi\mathrm{i}.\end{aligned} \tag{54}$$

It follows that the first Chern number for the bundle Λ_+ is defined and evaluated as

$$c_1 = \frac{\mathrm{i}}{2\pi}\int_{\mathbb{S}^2_N} F^+ = -1. \tag{55}$$

In the same manner, we find that the first Chern number c_1 for the eigenspace bundle Λ_- assocaited with $\lambda_-(\boldsymbol{N})$ equals 1.

A.2. **Index for a vector field.** The Chern number can be equally calculated locally through the index of the vector field. This is important for further applicaions to linearized problems.

Manipulation (54) is valid also when the equator $\mathbb{S}^1_N$ is deformed into a small circle $\Gamma(\theta_0)$ around the north pole with small constant latitude θ_0. In the limit $\theta_0 \to 0$, the integral of $\eta^{-1}\mathrm{d}\eta$ along $\Gamma(\theta_0)$ gives the index of a vector field locally defined in the neighbourhood of the north pole [21]. To see this, we take $(x, y) = (N_2, N_3)$ as local coordinates on the northern hemisphere. Then, we can view twice the upper right component N_- of H as a vector field $\boldsymbol{W} = (X, Y) = (N_2, -N_3)$ on the vicinity of the north pole, where $\boldsymbol{W}$ has a singular point (or vanishes) at the north pole. In terms of (X, Y), we rewrite η as

$$\eta = \frac{X + iY}{\sqrt{X^2 + Y^2}},$$

and further obtain

$$\eta^{-1}d\eta = i\frac{XdY - YdX}{X^2 + Y^2}.$$

Outside of the north pole, we denote the normalized $\boldsymbol{W}$ by $\boldsymbol{w}$ and define $\boldsymbol{v}$ to be the vector field $\boldsymbol{w}$ rotated counterclockwise by $\pi/2$,

$$\boldsymbol{w} = \frac{1}{\sqrt{X^2 + Y^2}}\begin{pmatrix} X \\ Y \end{pmatrix}, \quad \boldsymbol{v} = \frac{1}{\sqrt{X^2 + Y^2}}\begin{pmatrix} -Y \\ X \end{pmatrix}.$$

Then, the $\eta^{-1}d\eta$ is rewritten as

$$\eta^{-1}d\eta = i\boldsymbol{v}\cdot d\boldsymbol{w},$$

so that one obtains

$$\frac{1}{2\pi i}\int_{\Gamma(\theta_0)} \eta^{-1}d\eta = \frac{1}{2\pi}\int_{\Gamma(\theta_0)} \boldsymbol{v}\cdot d\boldsymbol{w}.$$

If we make θ_0 tend to zero, then the right-hand side of the above equation becomes the definition of the index of the vector field $\boldsymbol{W}$ at the singular point;

$$\mathrm{ind}(\boldsymbol{W}) = \lim_{\theta_0\to 0}\frac{1}{2\pi}\int_{\Gamma(\theta_0)} \boldsymbol{v}\cdot d\boldsymbol{w}.$$

In calculating the index, the linear approximation of $\boldsymbol{W}$ works well. In fact, we see that

$$\mathrm{Ind}(\boldsymbol{W}) = \begin{cases} 1 & \text{if } \det A > 0, \\ -1 & \text{if } \det A < 0, \end{cases} \qquad A = \begin{pmatrix} \frac{\partial X}{\partial x} & \frac{\partial X}{\partial y} \\ \frac{\partial Y}{\partial x} & \frac{\partial Y}{\partial y} \end{pmatrix}, \tag{56}$$

where A is the Jacobi matrix evaluated at the origin $(x, y) = (0, 0)$. For the vector field $\boldsymbol{W} = (N_2, -N_3)$, one has

$$A = \begin{pmatrix} 1 & 0 \\ 0 & -1 \end{pmatrix},$$

so that $\mathrm{ind}(\boldsymbol{W}) = -1$. It then turns out that

$$c_1 = \frac{i}{2\pi}\int_{\mathbb{S}^2_N} F^+ = \mathrm{Ind}(\boldsymbol{W}) = -1. \tag{57}$$

Eqs. (56) and (57) are put together to show that the Chern number c_1 is determined through the linearization of the Hamiltonian at the exceptional point for the eigenvector.

So far we have taken a small circle around the north pole. We may equally take a small circle around the south pole. In the southern hemisphere, we have to take $(x, y) = (N_3, N_2)$ as local coordinates on account of the orientation of the sphere. In this setting, the locally defined vector field determined by twice the upper-right component N_- is given by $\boldsymbol{W}' = (X', Y') = (-N_3, N_2)$, where X' and Y' are the imaginary and the real parts of N_-. Then, the Jacobi matrix evaluated at the south pole is

$$\begin{pmatrix} \frac{\partial X'}{\partial x} & \frac{\partial X'}{\partial y} \\ \frac{\partial Y'}{\partial x} & \frac{\partial Y'}{\partial y} \end{pmatrix} = \begin{pmatrix} -1 & 0 \\ 0 & 1 \end{pmatrix},$$

so that we obtain $\mathrm{Ind}(\boldsymbol{W}') = -1$, the same as $\mathrm{Ind}(\boldsymbol{W})$.

In the above discussion, we assume a sole exceptional point at the north or the south pole. If an eigenvector has several exceptional points, we have to linearize the Hamiltonian at every such point and to sum up the respective indices in order to obtain the Chern number c_1.

A.3. **Delta-Chern calculation in the non-compact setting.** We now look into the linearized Hamiltonian at the north pole of $\mathbb{S}^2(N)$. Associating the Poisson algebra so(3) of angular momenta $\boldsymbol{N}$ with the $\boldsymbol{N}$-space $\mathbb{R}^3_{\boldsymbol{N}}$, we obtain a Poisson manifold with $\mathbb{S}^2(N)$ as its symplectic submanifold. The Poisson commutation relation $\{N_2, N_3\} = N_1$ for fixed $N > 0$ gives rise to

$$\left\{\frac{N_2}{\sqrt{N}}, \frac{N_3}{\sqrt{N}}\right\} = \frac{N_1}{N}.$$

Then, on the tangent plane to $\mathbb{S}^2_N$ at the north pole $\{N_1 = N\}$, we can introduce canonical variables by

$$q = \frac{N_2}{\sqrt{N}}, \quad p = \frac{N_3}{\sqrt{N}}.$$

Rewriting the initial Hamiltonian as

$$H = \sqrt{\frac{N}{2}}\begin{pmatrix} \sqrt{\frac{N}{2}}\frac{N_1}{N} & \frac{N_-}{\sqrt{2}\sqrt{N}} \\ \frac{N_+}{\sqrt{2}\sqrt{N}} & -\sqrt{\frac{N}{2}}\frac{N_1}{N} \end{pmatrix} \tag{58}$$

and rescaling by $\sqrt{\frac{N}{2}}$, we obtain the linearized Hamiltonian

$$K_\mu = \begin{pmatrix} \mu & \frac{q-ip}{\sqrt{2}} \\ \frac{q+ip}{\sqrt{2}} & -\mu \end{pmatrix}, \quad \mu = \sqrt{\frac{N}{2}}. \tag{59}$$

Although μ is a positive number by the initial definition, we will treat μ as a parameter taking values in $\mathbb{R}$. At the same time, if we linearize the Hamiltonian at

the south pole $\{N_1 = -N\}$, we obtain

$$K'_\mu = \begin{pmatrix} -\mu & -i\frac{q+ip}{\sqrt{2}} \\ i\frac{q-ip}{\sqrt{2}} & \mu \end{pmatrix}. \tag{60}$$

The eigenvalues of K_μ

$$\nu_\pm = \pm\sqrt{\mu^2 + \frac{1}{2}(q^2+p^2)} \tag{61}$$

are degenerate if and only if $\mu = 0$ and $q = p = 0$. The eigenvectors associated with ν_+ are expressed in two ways as

$$|v^+_{\rm up}\rangle = \frac{1}{M^+_{\rm up}}\begin{pmatrix} (q-ip)/\sqrt{2} \\ \nu_+ - \mu \end{pmatrix}, \quad M^+_{\rm up} = \sqrt{2\nu_+(\nu_+ - \mu)}, \tag{62a}$$

$$|v^+_{\rm down}\rangle = \frac{1}{M^+_{\rm down}}\begin{pmatrix} \nu_+ + \mu \\ (q+ip)/\sqrt{2} \end{pmatrix}, \quad M^+_{\rm down} = \sqrt{2\nu_+(\nu_+ + \mu)}, \tag{62b}$$

where the domains of $|v^+_{\rm up/down}\rangle$ are, respectively,

$$V^+_{\rm up} = \begin{cases} \mathbb{R}^2 \setminus \{0\} & \text{if } \mu > 0, \\ \mathbb{R}^2 & \text{if } \mu < 0, \end{cases} \quad V^+_{\rm down} = \begin{cases} \mathbb{R}^2 & \text{if } \mu > 0, \\ \mathbb{R}^2 - \{0\} & \text{if } \mu < 0. \end{cases} \tag{63}$$

On the intersection $V^+_{\rm up} \cap V^+_{\rm down}$, the eigenvectors $|v^+_{\rm up/down}\rangle$ are related by

$$|v^+_{\rm up}\rangle = |v^+_{\rm down}\rangle\zeta, \quad \zeta = \frac{q-ip}{\sqrt{q^2+p^2}}. \tag{64}$$

In what follows, we show that delta-Chern δc_1, a change in the formal Chern number c_1 for the linearized Hamiltonian with non-compact phase space [24], provides the exact value of the Chern number for the semi-quantum eigenstate bundles of the initial Hamiltonian (46). The main step here is the calculation of δc_1 for non-compact setting where it appears as a mapping degree. To simplify our notation, we introduce variables

$$\boldsymbol{k} = (k_1, k_2) = (q,p)/\sqrt{2}.$$

Then, the model Hamiltonian K_μ with non-compact phase space $\mathbb{R}^2_{\boldsymbol{k}}$ is expressed as

$$K_\mu = \begin{pmatrix} \mu & k_1 - {\rm i}k_2 \\ k_1 + {\rm i}k_2 & -\mu \end{pmatrix}, \quad \boldsymbol{k} \in \mathbb{R}^2, \tag{65}$$

and eq. (64) is rewritten as

$$|v^+_{\rm up}(\boldsymbol{k})\rangle = \zeta\,|v^+_{\rm down}(\boldsymbol{k})\rangle, \quad \text{with } \zeta = \frac{k_1 - {\rm i}k_2}{k}, \quad k := \|\boldsymbol{k}\| = \sqrt{k_1^2 + k_2^2}. \tag{66}$$

This relation determines the complex line bundle associated with ν_+, which we call the eigen-line bundle and denote by L^+.

Local connection forms $B^+_{\rm up}$ and $B^+_{\rm down}$ for L^+ are defined to be

$$B^+_{\rm up} = \langle v^+_{\rm up}(\boldsymbol{k})|d|v^+_{\rm up}(\boldsymbol{k})\rangle, \quad B^+_{\rm down} = \langle v^+_{\rm down}(\boldsymbol{k})|d|v^+_{\rm down}(\boldsymbol{k})\rangle, \tag{67}$$

respectively. From (66), they are shown to be related by

$$B^+_{\rm up} - B^+_{\rm down} = \zeta^{-1}d\zeta, \tag{68}$$

where it is to be noted that this relation is independent of μ. The curvature form G^+ is globally defined on $\mathbb{R}^2$ and evaluated as

$$G^+ = dB^+_{\rm up} = dB^+_{\rm down} = \frac{\rm i}{2}\frac{\mu\, dk_1 \wedge dk_2}{(k^2+\mu^2)^{3/2}}. \tag{69}$$

The Chern number can be formally defined and evaluated, by using (69), as

$$\frac{\mathrm{i}}{2\pi}\int_{\mathbb{R}^2} G^+ = -\frac{1}{2}\,\mathrm{sgn}(\mu). \tag{70}$$

While the formal Chern number (70) is not integer-valued, the difference between the formal Chern number for $\mu > 0$ and that for $\mu < 0$ takes an integer value,

$$\frac{i}{2\pi}\int_{\mathbb{R}^2} G^+|_{\mu>0} - \frac{i}{2\pi}\int_{\mathbb{R}^2} G^+|_{\mu<0} = -1,$$

which is the same value as in Eq. (57).

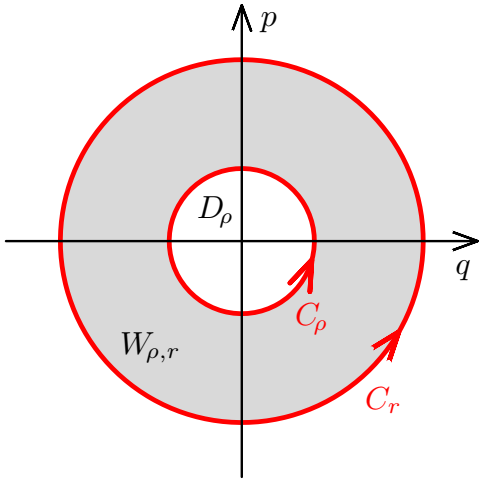

FIGURE 11. Circles C_ρ and C_r of respective radii ρ and r form the boundary of the annulus $W_{\rho,r}$, and C_ρ is also the boundary of disk D_ρ.

In what follows, we show that the difference makes sense as a topological quantity. For $\mu > 0$, the origin $\boldsymbol{k} = 0$ is the exceptional point for $|v^+_{\mathrm{up}}(\boldsymbol{k})\rangle$ but not so for $|v^+_{\mathrm{down}}(\boldsymbol{k})\rangle$. With this in mind, we integrate the curvature form G^+ on the regions D_ρ and $W_{\rho,r}$ shown in Fig. 11 to obtain

$$\begin{aligned}\int_{\mathbb{R}^2} G^+ &= \int_{D_\rho} dB^+_{\mathrm{down}} + \lim_{r\to\infty}\int_{W_{\rho,r}} dB^+_{\mathrm{up}} \\ &= \int_{C_\rho} B^+_{\mathrm{down}} + \lim_{r\to\infty}\Big(\int_{-C_\rho} B^+_{\mathrm{up}} + \int_{C_r} B^+_{\mathrm{up}}\Big) \\ &= -\int_{C_\rho} \zeta^{-1}d\zeta + \lim_{r\to\infty}\int_{C_r} B^+_{\mathrm{up}} \quad \text{for } \mu > 0,\end{aligned} \tag{71}$$

where use has been made of the relation (68) and the Stokes theorem. For $\mu < 0$, the origin is the exceptional point of $|v^+_{\mathrm{down}}(\boldsymbol{k})\rangle$ but not so for $|v^+_{\mathrm{up}}(\boldsymbol{k})\rangle$. A similar calculation to the above provides

$$\int_{\mathbb{R}^2} G^+ = \int_{C_\rho} \zeta^{-1}d\zeta + \lim_{r\to\infty}\int_{C_r} B^+_{\mathrm{down}} \quad \text{for } \mu < 0. \tag{72}$$

Although eqs. (71) and (72) contain locally-defined terms, $B^+_{\rm up}$ and $B^+_{\rm down}$, their difference may give a characteristics of the eigen-line bundle L^+ depending on μ. In fact, using (68) and the equality $\int_{C_r}\zeta^{-1}d\zeta=\int_{C_\rho}\zeta^{-1}d\zeta$, one can verify that

$$\frac{\mathrm{i}}{2\pi}\int_{\mathbb{R}^2}G^+\big|_{\mu>0}-\frac{\mathrm{i}}{2\pi}\int_{\mathbb{R}^2}G^+\big|_{\mu<0}=-\frac{\mathrm{i}}{2\pi}\int_{C_\rho}\zeta^{-1}\mathrm{d}\zeta\ . \tag{73}$$

Equation (73) implies that a jump δc_1 in the formal Chern number accompanying the variation of the parameter μ is a topological invariant which is given by the winding number associated with the mapping defined through the transition function $\zeta : C_\rho \to U(1)$. We note also that (73) holds for any μ-independent function ζ.

A.4. **Delta-Chern as the index of the Δ-bundle.** We turn to the relation between the delta-Chern index δc_1 which is introduced in eq. (73) of sec. A.3 and the index c_1 of the eigenvector bundle Δ over the sphere $\mathbb{S}^2$ surrounding the origin in the parameter space. The Δ bundle arises naturally in all geometric phase systems [38, 5, 43] when no distinction of control parameters as dynamical and formal (sec. 1.1) is made. The relation of the two indices is suggested in sec. 1.2 and is further discussed and exploited in the analysis of concrete systems, notably in sec. 2.2, sec. 3.1.1 and footnote 10, secs. 4.3 and 5.3. In this section, we uncover this relation explicitly using the results of sec. A.1 and A.3.

Let us consider a generic semi-quantum 2×2 Hermitian matrix Hamiltonian H_m with one tuning control parameter $m\in\mathbb{R}$ and dynamical control parameters defining points $\boldsymbol{p}$ on a two-dimensional classical phase space P of the slow subsystem. The total parameter space $\mathbb{R}\times P$ is of dimension 3. The eigenvalues $\lambda_{1,2}$ of H_m are functions $\mathbb{R}\times P\to\mathbb{R}$. In a generic system, they become degenerate [41, 1] at isolated points $\zeta_0=(m_0,\boldsymbol{p}_0)$ of $\mathbb{R}\times P$. Let us assume that $\lambda_{1,2}$ become degenerate for $m_0=0$. If other isolated non-regular values of m exist, we can always work on a sufficiently small open regular neighbourhood $M\ni 0$, otherwise $M=\mathbb{R}$. Similarly, we can always work on an open neighbourhood of $\boldsymbol{p}_0\in P$ where $\boldsymbol{p}_0$ remains a unique degeneracy point, but for simplicity, let us assume for now that $\boldsymbol{p}_0$ is unique on P. Shifting energy by $\lambda_0(m,\boldsymbol{p})=\frac{1}{2}(\lambda_1+\lambda_2)$ can always make H_m traceless on $M\times P$. Since $\lambda_{1,2}$ remain distinct on $M\setminus 0$, the adjusted eigenvalues λ_+ and λ_- are strictly positive and strictly negative on $(M\times P)\setminus\zeta_0$ and become 0 in the degeneracy point ζ_0. At the same time, the derivatives $\partial\lambda_\pm/\partial(m,\boldsymbol{p})\big|_{\zeta_0}$ do not vanish in a typical system [1]. Consequently, the linearization of H_m at ζ_0 is of the type (1) with ζ_0-specific parameters $\boldsymbol{B}(\zeta_0)$. Furthermore, for a sufficiently general physical interaction between the two dynamical subsystems, this linearization results in a Dirac-oscillator-type system (sec. 2.2) with local symplectic coordinates (q,p) on $\mathbb{R}^2_{q,p}=T_{\boldsymbol{p}_i}P$, $\{q,p\}=1$. Sections 3.2 and 4.2 provide concrete illustrations.

For each regular $m\in M\setminus 0$, the eigenvectors corresponding to eigenvalues $\lambda_{1,2}$ of H_m form two rank-1 complex line bundles over P, which we refer to as *eigenvector or eigenstate bundles*, and which we denote $\Lambda_{1,2}$ in sec. 1.2 and in the rest of the article. Since the Chern number of the combined rank-2 bundle Λ over P, or the *eigenspace bundle*, remains unchanged for all $m\in M$, it suffices to study one of the $\Lambda_{1,2}$ components. In what follows, we will assume that H_m is (made) traceless, and adapting the more informative $\pm$ notation, we will work with the Λ_+ bundle. Λ_+ constitutes two *continuous* one-parameter families of bundles $\Lambda_{+,m<0}$ and $\Lambda_{+,m>0}$. In other words, bundles $\Lambda_{+,m}$ over P have a certain fixed topology

on each disconnected component of $M \setminus 0$. The delta-Chern index δc_1 characterizes the change of this topology at $m = 0$. For a compact P (with sole point $\boldsymbol{p}_0$), this index can be computed simply as

$$\delta c_1(\Lambda_+) = c_1(\Lambda_{+,m>0}) - c_1(\Lambda_{+,m<0}). \tag{74}$$

In the non-compact setting, we can either use formal Chern numbers (70) [21, 23] or rely directly on (73). Since (73) defines a local number its application does, generally, require linearization at ζ_0.

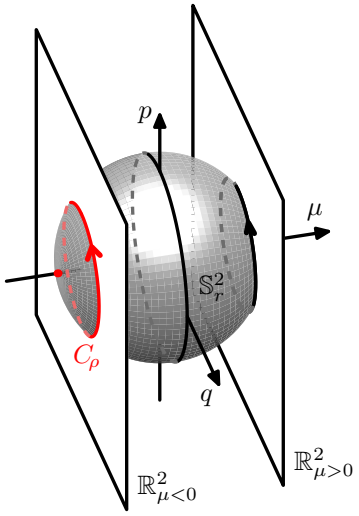

FIGURE 12. Base spaces $\mathbb{R}^2_\mu$ and $\mathbb{S}^2_r$ of the $\Lambda_\pm$ and $\Delta_\pm$ eigenvector bundles, respectively, in the parameter space $\mathbb{R}^3$ of the Dirac oscillator (sec. 2.2). The spaces intersect on the $\mathbb{S}^1$ circle C_ρ involved in the Chern index calculus, see sec. A.4 for details, and compare to fig 11.

At the same time, we consider *local eigenvector bundles* Δ_+ over sphere $\mathbb{S}^2_{r,\zeta_0}$ of sufficiently small radius r surrounding ζ_0 in the combined control parameter space $M \times P$. In this space, as illustrated in fig. 12, typical non-empty intersections of P and $\mathbb{S}^2_{r,\boldsymbol{p}_i}$ are circles of radius $\rho = (r^2 - m^2)^{1/2} > 0$

$$C_{\rho,m} := \mathbb{S}^1_\rho = (m, P) \cap \mathbb{S}^2_{r,\zeta_0} \quad \text{with fixed } m,\ |m| < r. \tag{75}$$

Indeed, the existence of $\partial\lambda/\partial\boldsymbol{p}$ at $\boldsymbol{p}_0$ already requires that $\boldsymbol{p}_0$ is contained in P together with an open saturated disk $D_\epsilon = \{\boldsymbol{p} \in P; \|\boldsymbol{p}_0 - \boldsymbol{p}\| < \epsilon\}$ of some, possibly small, finite radius $\epsilon > 0$. Taking $r < \epsilon$, we make sure that $\mathbb{S}^2_{r,\zeta_0} \subset M \times P$ and consequently, that typical non-empty constant-m sets $C_{\rho,m}$ on $\mathbb{S}^2_{r,\zeta_0}$ lie entirely within D_ϵ. We have seen across sec. A.1 and A.3 that Chern and delta-Chern numbers c_1 and δc_1 of line bundles Λ_+ are computed (for fixed regular values of the tuning parameter m) using integrals (54) and (73) over certain circles in the base space P. This makes $C_{\rho,m}$ central to our analysis here.

Consider the Δ and Λ bundles of the Dirac oscillator (sec. 2.2), the most basic typical 2×2 semi-quantum system. It has traceless Hamiltonian (11) with tuning control parameter $\mu \in M = \mathbb{R}$ and dynamical control parameters $(q, p) \in P = \mathbb{R}^2$.

Its eigenvalues have a sole degeneracy point $\boldsymbol{p}_0 = (0,(0,0))$. The following lemma lays the corner stone of our analysis.

Lemma A.1 (δc_1 and $c_1(\Delta)$ in the noncompact local setup)**.** *The Chern number c_1 of the local eigenvalue bundle Δ_+ of the Dirac oscillator (sec. 2.2) equals the delta-Chern index δc_1 of its one-parameter family of bundles $\Lambda_{+,\mu}$,*

$$c_1(\Delta_+) = \delta c_1(\Lambda_+) = 1 \ .$$

Proof. As pointed out in sec. 2.2, the local bundle Δ of the Dirac oscillator can be identified with that of the Berry spin system (1) and of the spin-orbit system (2)–(4)–(46) through a simple GL(3) parameter rescaling

$$\left(2\mu, \sqrt{2}q, -\sqrt{2}p\right) \mapsto \boldsymbol{B} \mapsto \boldsymbol{N}.$$

Since the determinant of this map (cf. [25, eq. (107)]) is negative, the index (55) and the Chern number $c_1(\Delta_+)$ are of opposite signs, i.e.,

$$c_1(\Delta_+) = 1 \ .$$

Further comparing to sec. A.1, we note that now the radius of the base space $\mathbb{S}^2_N$ becomes r, and that the transition function in (50) equals

$$\eta = \frac{q + \mathrm{i}p}{\sqrt{q^2+p^2}} = \exp(\mathrm{i}\varphi) \quad \text{with } \varphi = \arg(q+\mathrm{i}p) = -\phi \ .$$

As pointed out in sec. A.2, the integration (54) may follow any constant level set of $N_1 = 2\mu$ with $|2\mu| < r$, such as

$$C_\rho = \mathbb{S}^1_\rho \subset \mathbb{R}^2_{\mu<0} \cap \mathbb{S}^2_r = \left\{(\mu,q,p);\ 2\,(q^2+p^2) = \rho^2,\ 2\,\mu = -\sqrt{r^2-\rho^2}\right\}$$

shown in fig. 12. Comparing to the delta-Chern computation in sec. A.3, we note that its matrix Hamiltonian (59) is made identical to (11) through

$$(\mu,q,p) \mapsto \left(-\sqrt{2}\mu, -q, -p\right).$$

It follows that (73) and the delta-Chern of (11) are of opposite signs, i.e.,

$$\delta c_1(\Lambda_+) = 1 \ .$$

In more detail, we can see that in our coordinates, the transition function

$$\zeta = -\frac{q - \mathrm{i}p}{\sqrt{q^2+p^2}} = -\frac{1}{\eta}$$

differs in sign from its original form in (64) while the direction on C_ρ is preserved. The sign gets trivially cancelled in (73). On the other hand, the inversion of the parameter space $\mathbb{R}^3$, which can be seen otherwise as flipping the energy-axis, is important. The positive-energy bundle Λ_+ of (59) corresponds to the negative-energy bundle Λ_- of the Dirac oscillator (11). Therefore, computing the delta-Chern number for the Λ_+ bundle of (11), we should use (73) with an additional factor of -1

$$\delta c_1(\Lambda_+) = \frac{\mathrm{i}}{2\pi}\int_{C_\rho} \zeta^{-1}\mathrm{d}\zeta = \frac{\mathrm{i}}{2\pi}\int_{C_\rho} \eta\,\mathrm{d}\eta^{-1} = \frac{1}{2\pi}\int_{C_\rho}\mathrm{d}\varphi = 1 \ . \qquad \square$$

A similar lemma can be formulated and proven for systems with compact phase space P. We turn to the particular system in sec. 3 with $P = \mathbb{S}^2_N$ and tuning control

parameter $\gamma \in (0,1)$ because, like the Dirac oscillator in lemma A.1, it has a sole degeneracy point

$$(\gamma, \boldsymbol{p}_0) = \left(\tfrac{1}{2}, (-N,0,0)\right) \in [0,1] \times \mathbb{S}^2_N \ .$$

Lemma A.2 (δc_1 and $c_1(\Delta)$ in the compact local setup)**.** *The Chern number c_1 of the local bundle Δ_+ of the basic spin-orbit system in sec. 3 with tuning and dynamical control parameters $\gamma \in [0,1]$ and $\boldsymbol{p} = \{\boldsymbol{N}, \|\boldsymbol{N}\| = N\} \in \mathbb{S}^2_N$, respectively, equals the delta-Chern index δc_1 of its one-parameter family of bundles $\Lambda_{+,\gamma}$ over $\mathbb{S}^2_N$.*

Proof. The Chern numbers $c_1(\Lambda_\pm)$ equal zero for $\gamma = 0$ and are computed in sec. A.1 for $\gamma = 1$. Continuing from these limits, we find $\delta c_1(\Lambda_+) = -1 - 0 = -1$. We can also rely on sec. A.1 and footnote 10 to compute $c_1(\Delta_+)$ like we did in the proof of lemma A.1. The circle $C_\rho = \mathbb{S}^2_{N,\mu<0} \cap \mathbb{S}^2_{(\mu,N_2,N_3)}$ parameterized by (N_2, N_3) is at the centre of the analysis. Omitting the details, $c_1(\Delta_+) = -1$. □

Remark 1 (linearization)**.** By itself, lemma A.2 does not imply any linearization of the semi-quantum Hamiltonian H_γ defined on $\mathbb{S}^2_N$. However, the radius $r < N$ of the base space $\mathbb{S}^2_r$ of the local bundle Δ can be chosen sufficiently small $r \ll N$ for linearizing H_γ at the degeneracy point $\boldsymbol{N} = (-N,0,0)^T$ to be viable (see sec. 3.2) and for the Chern index computation to take advantage of such linearization. Delta-Chern δc_1 can as well be defined and computed locally at the $(-N,0,0)$ pole using the linearization approach in sec. A.3.

It remains to address the situation with several equivalent isolated degeneracy points $(0,\boldsymbol{p}_i)$ on $(0,P)$ where $\lambda_{1,2}$ attain the same value. The existence of such points may be related to the presence of symmetries $P \to P$ or, more generally, of a nontrivial isotropy group $\mathrm{Diff}(P)$ whose operations leave H_m invariant, see sec. 4 and [25] for the concrete examples. In a sufficiently small open neighbourhood of each $(0,\boldsymbol{p}_i)$, the system is generic in the sense of [41, 1] and our lemmas apply. Following the ideas in sec. A.2, we can sum the Chern numbers c_1 of the local bundles $\Delta_{+,i}$ in order to match the delta-Chern $\delta c_1(\Lambda_+)$ for the bundle Λ_+ over the entire P.

A.5. **Spin-orbit coupling Hamiltonian in the presence of a magnetic field.** We calculate here the Chern numbers for semi-quantum Hamiltonian (22) using the matrix representation (24) in the basis $\{|\frac{1}{2},\frac{1}{2}\rangle, |\frac{1}{2},-\frac{1}{2}\rangle\}$ and with parameter γ replaced by parameter t

$$H_t = (1-t)\begin{pmatrix} 1 & 0 \\ 0 & -1 \end{pmatrix} + \frac{t}{N}\begin{pmatrix} N_1 & N_- \\ N_+ & -N_1 \end{pmatrix}, \quad 0 \le t \le 1. \tag{76}$$

The eigenvalues (26) of H_t

$$\lambda_\pm = \pm\sqrt{1 - 2t(1-t)(1-N_1/N)}, \tag{77}$$

are degenerate if and only if $N_1 = -N$ and $t = \frac{1}{2}$. The eigenvector associated with λ_+ can be expressed in two ways as

$$|u^+_{\mathrm{up}}\rangle = \frac{1}{N^+_{\mathrm{up}}}\begin{pmatrix} tN_-/N \\ \lambda_+ - 1 + t - tN_1/N \end{pmatrix} \text{ and} \tag{78a}$$

$$|u^+_{\mathrm{down}}\rangle = \frac{1}{N^+_{\mathrm{down}}}\begin{pmatrix} \lambda_+ + 1 - t + tN_1/N \\ tN_+/N \end{pmatrix}, \tag{78b}$$

where the normalization factors $N^+_{\text{up/down}}$ are given, respectively, by

$$N^+_{\text{up}} = \sqrt{2\lambda_+(\lambda_+ - 1 + t(1 - N_1/N))} \text{ and} \tag{79a}$$

$$N^+_{\text{down}} = \sqrt{2\lambda_+(\lambda_+ + 1 - t(1 - N_1/N))}. \tag{79b}$$

The exceptional points at which definitions (78) fail are listed below

t	$0 \le t < \frac{1}{2}$	$\frac{1}{2} < t \le 1$
excep. pts. of $\lvert u^+_{\text{up}}\rangle$	$\{N_1 = \pm N\}$	$\{N_1 = N\}$
excep. pts. of $\lvert u^+_{\text{down}}\rangle$	$\emptyset$	$\{N_1 = -N\}$

, (80)

where $\{N_1 = N\}$ and $\{N_1 = -N\}$ denote the north and the south poles of the two-sphere $\mathbb{S}^2_N$ of radius N.

According to (80), the eigenvector $|u^+_{\text{down}}\rangle$ is globally defined on $\mathbb{S}^2_N$ for $0 \le t < \frac{1}{2}$, so that the eigenvector bundle Λ_+ associated with λ_+ is trivial. On the contrary, for $\frac{1}{2} < t \le 1$, both eigenvectors $|u^+_{\text{up/down}}\rangle$ are only locally defined, which means that Λ_+ is non-trivial. It follows that the topology of Λ_+ changes when the control parameter t passes the critical value $\frac{1}{2}$. Since the Chern number c_1 is piecewise constant in t, it suffices to evaluate c_1 for $t = 0$ and $t = 1$. For $t = 0$, the Chern number is, of course, $c_1 = 0$. For $t = 1$, we have already evaluated the Chern number $c_1 = -1$ for the eigenvector bundle associated with λ_+.

A.6. **A family of $\mathcal{T}$-invariant Hamiltonians H_α.** In this section, we work with the semi-quantum Hamiltonian (31) written in the matrix representation (32) with the basis $\{|\frac{1}{2}, \frac{1}{2}\rangle, |\frac{1}{2}, -\frac{1}{2}\rangle\}$

$$H_\alpha = \frac{\alpha}{N}\begin{pmatrix} N_1 & N_- \\ N_+ & -N_1 \end{pmatrix} - i\frac{\varepsilon}{N}\begin{pmatrix} 0 & N_- \\ -N_+ & 0 \end{pmatrix}, \quad -1 \le \alpha \le 1, \tag{81}$$

where $0 < |\varepsilon| < 1$ is a small non-zero constant. The eigenvalues (33) of H_α

$$\lambda_\pm = \pm\sqrt{\alpha^2 + \varepsilon^2 \sin^2\theta}, \tag{82}$$

where (θ, ϕ) are spherical coordinates on $\mathbb{S}^2_N$, become degenerate if and only if

$$\alpha = 0, \quad \theta = 0, \pi. \tag{83}$$

For $\alpha \neq 0$, the eigenvectors associated with λ_+ are expressed in two ways as

$$|u^+_{\text{up}}\rangle = \frac{1}{N^+_{\text{up}}}\begin{pmatrix} (\alpha - i\varepsilon)e^{-i\phi}\sin\theta \\ \lambda_+ - \alpha\cos\theta \end{pmatrix} \text{ and} \tag{84a}$$

$$|u^+_{\text{down}}\rangle = \frac{1}{N^+_{\text{down}}}\begin{pmatrix} \lambda_+ + \alpha\cos\theta \\ (\alpha + i\varepsilon)e^{i\phi}\sin\theta \end{pmatrix}, \tag{84b}$$

where the normalization factors $N^+_{\text{up/down}}$ are given, respectively, by

$$N^+_{\text{up}} = \sqrt{2\lambda_+(\lambda_+ - \alpha\cos\theta)} \quad \text{and} \quad N^+_{\text{down}} = \sqrt{2\lambda_+(\lambda_+ + \alpha\cos\theta)}\,. \tag{85}$$

The exceptional points at which the eigenvectors fail to be defined are as follows

α	$\alpha < 0$	$\alpha > 0$
exc. pts. of $\lvert u^+_{\text{up}}\rangle$	$\{N_1 = -N\}$	$\{N_1 = N\}$
exc. pts. of $\lvert u^+_{\text{down}}\rangle$	$\{N_1 = N\}$	$\{N_1 = -N\}$

(86)

In other words, the domains of $|u^+_{\mathrm{up/down}}\rangle$ are $\mathbb{S}^2_N$ without the respective exceptional points. On the intersection of those domains, the eigenvectors are related by

$$|u^+_{\mathrm{up}}\rangle = |u^+_{\mathrm{down}}\rangle\eta, \quad \eta = \frac{\alpha - i\varepsilon}{\sqrt{\alpha^2+\varepsilon^2}}e^{-i\phi}. \tag{87}$$

The local connection forms $A^+_{\mathrm{up/down}}$ are defined to be

$$A^+_{\mathrm{up}} = \langle u^+_{\mathrm{up}}|d|u^+_{\mathrm{up}}\rangle, \quad A^+_{\mathrm{down}} = \langle u^+_{\mathrm{down}}|d|u^+_{\mathrm{down}}\rangle. \tag{88}$$

Combining eq. (87) and the above definition yields the relation

$$A^+_{\mathrm{up}} = A^+_{\mathrm{down}} + \eta^{-1}\mathrm{d}\eta\ . \tag{89}$$

The local curvature forms are defined to be

$$F^+_{\mathrm{up}} = \mathrm{d}A^+_{\mathrm{up}} \quad \text{and} \quad F^+_{\mathrm{down}} = \mathrm{d}A^+_{\mathrm{down}}. \tag{90}$$

On account of (89), one has $F^+_{\mathrm{up}} = F^+_{\mathrm{down}}$, so that the curvature form F^+ is globally defined on $\mathbb{S}^2_N$. We integrate the curvature form F^+ over $\mathbb{S}^2_N$ both for $\alpha < 0$ and $\alpha > 0$. In the case of $\alpha < 0$, after dividing $\mathbb{S}^2_N$ into the north hemisphere $\mathbb{S}^2_{N+}$ and the south hemisphere $\mathbb{S}^2_{N-}$, the integration is performed as follows:

$$\begin{aligned}\int_{\mathbb{S}^2_N} F^+ &= \int_{\mathbb{S}^2_{N-}} F^+_{\mathrm{down}} + \int_{\mathbb{S}^2_{N+}} F^+_{\mathrm{up}} = \int_{\mathbb{S}^2_{N-}} dA^+_{\mathrm{down}} + \int_{\mathbb{S}^2_{N+}} dA^+_{\mathrm{up}} \\ &= -\int_{\mathbb{S}^1_N} A^+_{\mathrm{down}} + \int_{\mathbb{S}^1_N} A^+_{\mathrm{up}} = \int_{\mathbb{S}^1_N} (A^+_{\mathrm{up}} - A^+_{\mathrm{down}}) \\ &= \int_{\mathbb{S}^1_N} \eta^{-1} d\eta = -2\pi i,\end{aligned}$$

where $\mathbb{S}^1_N$ denotes the equator of $\mathbb{S}^2_N$ and where the Stokes theorem and eq. (89) have been used. It then follows that the first Chern number for the eigenvector bundle Λ_+ associated with λ_+ is given by

$$c^+_1 = \frac{\mathrm{i}}{2\pi}\int_{\mathbb{S}^2_N} F^+ = +1 \quad \text{for } \alpha < 0. \tag{91}$$

In the case of $\alpha > 0$, calculation runs in parallel to give

$$\begin{aligned}\int_{\mathbb{S}^2_N} F^+ &= \int_{\mathbb{S}^2_{N-}} F^+_{\mathrm{up}} + \int_{\mathbb{S}^2_{N+}} F^+_{\mathrm{down}} = \int_{\mathbb{S}^2_{N-}} dA^+_{\mathrm{up}} + \int_{\mathbb{S}^2_{N+}} dA^+_{\mathrm{down}} \\ &= -\int_{\mathbb{S}^1_N} A^+_{\mathrm{up}} + \int_{\mathbb{S}^1_N} A^+_{\mathrm{down}} = -\int_{\mathbb{S}^1_N} (A^+_{\mathrm{up}} - A^+_{\mathrm{down}}) \\ &= -\int_{\mathbb{S}^1_N} \eta^{-1} d\eta = 2\pi\mathrm{i},\end{aligned}$$

It then follows that

$$c^+_1 = \frac{\mathrm{i}}{2\pi}\int_{\mathbb{S}^2_N} F^+ = -1 \quad \text{for } \alpha > 0. \tag{92}$$

In a similar manner, the Chern number for the eigenspace bundle Λ_- associated with the negative eigenvalue λ_- is evaluated to be

$$c_1^- = \frac{\mathrm{i}}{2\pi}\int_{\mathbb{S}^2_N} F^- = -1 \quad \text{for } \alpha < 0, \tag{93a}$$

$$c_1^- = \frac{\mathrm{i}}{2\pi}\int_{\mathbb{S}^2_N} F^- = +1 \quad \text{for } \alpha > 0. \tag{93b}$$

A.7. **Delta-Chern analysis for the linearized Hamiltonians.** We calculate now the Chern numbers for the time-reversal invariant semi-quantum Hamiltonians (36) and (36b). which correspond to the linearization of (32) at the north and south poles of the $\mathbb{S}^2_N$ sphere, respectively. We rewrite them using the $a^- = z = q + \mathrm{i}\,p$ representation as

$$K^{(+)}_\alpha = \begin{pmatrix} -\alpha & -\mathrm{i}\frac{(\alpha - i\varepsilon)}{\sqrt{N}} z \\ \mathrm{i}\frac{(\alpha + i\varepsilon)}{\sqrt{N}} \overline{z} & \alpha \end{pmatrix}, \tag{94a}$$

$$K^{(-)}_\alpha = \begin{pmatrix} \alpha & \frac{(\alpha - i\varepsilon)}{\sqrt{N}} \overline{z} \\ \frac{(\alpha + i\varepsilon)}{\sqrt{N}} z & -\alpha \end{pmatrix}, \tag{94b}$$

and find the eigenvalues of $K^{(+)}$

$$\nu_\pm = \pm\sqrt{\alpha^2 + \frac{\alpha^2 + \varepsilon^2}{N}|z|^2}\,. \tag{95}$$

The eigenvectors associated with ν_+ are expressed in two ways as

$$|v^{(+)}_{\mathrm{up}}\rangle = \frac{1}{N^{(+)}_{\mathrm{up}}} \begin{pmatrix} \frac{\alpha - i\varepsilon}{\sqrt{N}} \overline{z} \\ \nu_+ - \alpha \end{pmatrix}, \tag{96a}$$

$$|v^{(+)}_{\mathrm{down}}\rangle = \frac{1}{N^{(+)}_{\mathrm{down}}} \begin{pmatrix} \nu_+ + \alpha \\ \frac{\alpha + i\varepsilon}{\sqrt{N}} z \end{pmatrix}, \tag{96b}$$

where $N^{(+)}_{\mathrm{up/down}}$ are normalization factors given, respectively, by

$$N^{(+)}_{\mathrm{up}} = \sqrt{2\nu_+(\nu_+ - \alpha)}, \quad N^{(+)}_{\mathrm{down}} = \sqrt{2\nu_+(\nu_+ + \alpha)}. \tag{97}$$

The exceptional points at which the eigenvectors fail to be defined are listed as follows:

α	$\alpha < 0$	$\alpha > 0$
excep. pt. of $\lvert v^{(+)}_{\mathrm{up}}\rangle$	$\emptyset$	0
excep. pt. of $\lvert v^{(+)}_{\mathrm{down}}\rangle$	0	$\emptyset$

(98)

Outside of the exceptional points, the eigenvectors $|v^{(+)}_{\mathrm{up/down}}\rangle$ are related by

$$|v^{(+)}_{\mathrm{up}}\rangle = |v^{(+)}_{\mathrm{down}}\rangle\zeta, \quad \zeta = \frac{\alpha - i\varepsilon}{\sqrt{\alpha^2 + \varepsilon^2}}\frac{\overline{z}}{|z|}, \quad \overline{z} = q - ip. \tag{99}$$

The local connection forms are defined to be

$$B^{(+)}_{\mathrm{up}} = \langle v^{(+)}_{\mathrm{up}}|d|v^{(+)}_{\mathrm{up}}\rangle, \quad B^{(+)}_{\mathrm{down}} = \langle v^{(+)}_{\mathrm{down}}|d|v^{(+)}_{\mathrm{down}}\rangle, \tag{100}$$

and are related by

$$B^{(+)}_{\mathrm{up}} - B^{(+)}_{\mathrm{down}} = \zeta^{-1}d\zeta. \tag{101}$$

The local curvature forms are defined, accordingly, to be

$$G^{(+)} = dB^{(+)}_{\mathrm{up}} = dB^{(+)}_{\mathrm{down}}. \tag{102}$$

In the same manner as discussed in the subsection A.3, we obtain

$$\frac{i}{2\pi}\int_{\mathbb{R}^2} G^{(+)}|_{\alpha>0} - \frac{i}{2\pi}\int_{\mathbb{R}^2} G^{(+)}|_{\alpha<0} = \frac{1}{2\pi i}\int_C \zeta^{-1}d\zeta = -1. \tag{103}$$

We need further delta-Chern analysis for $K_\alpha^{(-)}$. The eigenvalues of $K_\alpha^{(-)}$ are easily evaluated as

$$\nu_\pm = \pm\sqrt{\alpha^2 + \frac{\alpha^2+\varepsilon^2}{N}|z|^2}. \tag{104}$$

The eigenvectors associated with ν_+ are expressed in two ways as

$$|v_{\rm up}^{(-)}\rangle = \frac{1}{N_{\rm up}^{(-)}}\begin{pmatrix} -i\frac{\alpha-i\varepsilon}{\sqrt{N}}z \\ \nu_+ + \alpha \end{pmatrix}, \tag{105a}$$

$$|v_{\rm down}^{(-)}\rangle = \frac{1}{N_{\rm down}^{(-)}}\begin{pmatrix} \nu_+ - \alpha \\ i\frac{\alpha+i\varepsilon}{\sqrt{N}}\overline{z} \end{pmatrix}, \tag{105b}$$

where $N_{\rm up/down}^{(-)}$ are the normalization factors given, respectively, by

$$N_{\rm up}^{(-)} = \sqrt{2\nu_+(\nu_+ + \alpha)}, \quad N_{\rm down}^{(-)} = \sqrt{2\nu_+(\nu_+ - \alpha)}. \tag{106}$$

The exceptional points at which the eigenvectors fail to be defined are listed as follows:

α	$\alpha < 0$	$\alpha > 0$
excep. pt. of $\lvert v_{\rm up}^{(-)}\rangle$	0	$\emptyset$
excep. pt. of $\lvert v_{\rm down}^{(-)}\rangle$	$\emptyset$	0

(107)

Outside of the exceptional points, the eigenvectors $|v_{\rm up/down}^{(-)}\rangle$ are related by

$$|v_{\rm up}^{(-)}\rangle = |v_{\rm down}^{(-)}\rangle\xi, \quad \xi = -i\frac{\alpha-i\varepsilon}{\sqrt{\alpha^2+\varepsilon^2}}\frac{z}{|z|}, \quad z = q + ip. \tag{108}$$

The local connection forms are defined to be

$$B_{\rm up}^{(-)} = \langle v_{\rm up}^{(-)}|d|v_{\rm up}^{(-)}\rangle, \quad B_{\rm down}^{(-)} = \langle v_{\rm down}^{(-)}|d|v_{\rm down}^{(-)}\rangle, \tag{109}$$

and are related by

$$B_{\rm up}^{(-)} - B_{\rm down}^{(-)} = \xi^{-1}d\xi. \tag{110}$$

The local curvature forms are defined, accordingly, to be

$$G^{(-)} = dB_{\rm up}^{(-)} = dB_{\rm down}^{(-)}. \tag{111}$$

In order to evaluate the delta-Chern, a similar method with small modification runs in parallel. For the sake of a review of the method, we reproduce the evaluation procedure. For $\alpha > 0$, the origin is the exceptional point for $|v_{\rm down}^{(-)}\rangle$ but not so for $|v_{\rm up}^{(-)}\rangle$. With this in mind, we integrate the curvature form $G^{(-)}$ on the regions D_ρ and $W_{\rho,r}$ shown in Fig. 11 to obtain

$$\begin{aligned}\int_{\mathbb{R}^2} G^{(-)} &= \int_{D_\rho} dB_{\rm up}^{(-)} + \lim_{r\to\infty}\int_{W_{\rho,r}} dB_{\rm down}^{(-)} \\ &= \int_{C_\rho} B_{\rm up}^{(-)} + \lim_{r\to\infty}\Big(\int_{-C_\rho} B_{\rm down}^{(-)} + \int_{C_r} B_{\rm down}^{(-)}\Big) \\ &= \int_{C_\rho} \xi^{-1}d\xi + \lim_{r\to\infty}\int_{C_r} B_{\rm down}^{(-)} \quad \text{for } \alpha > 0,\end{aligned} \tag{112}$$

where use has been made of the relation (110) and the Stokes theorem. For $\alpha < 0$, the origin is the exceptional point of $|v^+_{\rm up}\rangle$ but not so for $|v^+_{\rm down}\rangle$. A similar calculation to the above provides

$$\int_{\mathbb{R}^2} G^{(-)} = -\int_{C_\rho} \xi^{-1} d\xi + \lim_{r\to\infty} \int_{C_r} B^{(-)}_{\rm up} \quad \text{for } \alpha < 0. \tag{113}$$

Though Eqs. (112) and (113) contain locally-defined terms, $B^{(-)}_{\rm up}$ and $B^{(-)}_{\rm down}$, the difference between them may have a characteristic of the eigenvector bundle depending on α. In fact, one can verify that

$$\frac{i}{2\pi}\int_{\mathbb{R}^2} G^{(-)}\big|_{\alpha>0} - \frac{i}{2\pi}\int_{\mathbb{R}^2} G^{(-)}\big|_{\alpha<0} = \frac{-1}{2\pi i}\int_{C_\rho} \xi^{-1} d\xi = -1, \tag{114}$$

where use has been made of the relation (110) and the fact that $\int_{C_r} \xi^{-1} d\xi = \int_{C_\rho} \xi^{-1} d\xi$. Eqs. (103) and (114) imply that the respective jumps in the formal Chern number accompanying the variation of the parameter α make sense as topological invariants. For $\zeta : C_\rho \to U(1)$, it is a winding number, but for $\xi : C_\rho \to U(1)$, it is the negative of the winding number.

The Chern number of the eigenvector bundle associate with the positive eigenvalues of the initial Hamiltonian H_α is $c_1 = -1$ for $\alpha > 0$ and $c_1 = +1$ for $\alpha < 0$. Hence, the change in the Chern number in the positive direction of α is $-1 - (+1) = -2$. The initial semi-quantum Hamiltonian H_α has two degeneracy points at the north and the south poles of $\mathbb{S}^2_N$. We have evaluated the change in the formal Chern number for each of the linearized Hamiltonians. The totality of the change is $-1 + (-1) = -2$, the same result as above.

A.8. **Chern number calculation for spin-quadrupole Hamiltonian.** We begin with Hamiltonian (40) in the matrix form

$$H_\mu = \begin{pmatrix} \mu \mathsf{G} & \mathsf{M} \\ \mathsf{M}^\dagger & -\mu \mathsf{G} \end{pmatrix} \tag{115}$$

with tuning control parameter μ,

$$\mathsf{G} = \frac{N^2 - 3N_1^2}{2}\begin{pmatrix} 1 & 0 \\ 0 & -1 \end{pmatrix}, \text{ and } \mathsf{M} = \begin{pmatrix} (\sqrt{3}\mu + \mathrm{i}\varepsilon) N_1 N_+ & (\frac{1}{2}\sqrt{3} - \mathrm{i}\varepsilon) N_-^2 \\ (\frac{1}{2}\sqrt{3}\mu + \mathrm{i}\varepsilon) N_+^2 & -(\sqrt{3}\mu - \mathrm{i}\varepsilon) N_1 N_- \end{pmatrix}.$$

The eigenvalues of H_μ are

$$\lambda_\pm = \pm\sqrt{(\mu^2 + \varepsilon^2)N^2 - \varepsilon^2 N_3^2} = \pm N^2 \sqrt{\mu^2 + \varepsilon^2 \sin^2\theta}. \tag{116}$$

If $N \neq 0$, the degeneracy in eigenvalues takes place if and only if

$$\mu = 0, \quad \theta = 0, \quad \text{or} \quad \mu = 0, \quad \theta = \pi. \tag{117}$$

To simplify the analysis, we linearize Hamiltonian (115) at the north pole to obtain

$$N^2 \begin{pmatrix} -\mu & 0 & \beta z & 0 \\ 0 & -\mu & 0 & -\bar\beta \bar z \\ \bar\beta \bar z & 0 & \mu & 0 \\ 0 & -\beta z & 0 & \mu \end{pmatrix} \quad \text{with } \beta = \frac{\sqrt{3}\mu + \mathrm{i}\varepsilon}{\sqrt{N}}, \tag{118}$$

where

$$z = \frac{N_+}{\sqrt{N}} = q + \mathrm{i}p \quad \text{and} \quad \bar z = \frac{N_-}{\sqrt{N}} = q - \mathrm{i}p \tag{119}$$

are viewed as local coordinates on the tangent plane to $\mathbb{S}^2_N$ at the north pole. Rescaling by N^2 and reordering the basis functions as $\{|\frac{3}{2},\frac{3}{2}\rangle, |\frac{3}{2},\frac{1}{2}\rangle, |\frac{3}{2},-\frac{1}{2}\rangle, |\frac{3}{2},-\frac{3}{2}\rangle\}$ give the linearized semi-quantum Hamiltonian at the north pole

$$K_\mu = \begin{pmatrix} \mu & \bar\beta\bar z & & \\ \beta z & -\mu & & \\ & & -\mu & -\bar\beta\bar z \\ & & -\beta z & \mu \end{pmatrix}. \tag{120}$$

The analysis at the south pole can be done in a similar way, with two linearizations at the north and south poles being related through time-reversal transformation (6).

The eigenvalues of the linearized Hamiltonian (120)

$$\nu_\pm = \pm\sqrt{\mu^2 + |\beta|^2|z|^2} \tag{121}$$

have multiplicity 2 each and become totally degenerate if and only if $\mu = 0$ and $z = 0$. The normalized eigenvectors associated with ν_+ are expressed in two ways as

$$|w^+_{1,\mathrm{up}}\rangle = \frac{1}{N^+_{1,\mathrm{up}}}\begin{pmatrix} \bar\beta\bar z \\ \nu_+ - \mu \\ 0 \\ 0 \end{pmatrix}, \quad |w^+_{2,\mathrm{up}}\rangle = \frac{1}{N^+_{2,\mathrm{up}}}\begin{pmatrix} 0 \\ 0 \\ -\bar\beta\bar z \\ \nu_+ + \mu \end{pmatrix}, \tag{122a}$$

$$|w^+_{1,\mathrm{down}}\rangle = \frac{1}{N^+_{1,\mathrm{down}}}\begin{pmatrix} \nu_+ + \mu \\ \beta z \\ 0 \\ 0 \end{pmatrix}, \quad |w^+_{2,\mathrm{down}}\rangle = \frac{1}{N^+_{2,\mathrm{down}}}\begin{pmatrix} 0 \\ 0 \\ \nu_+ - \mu \\ -\beta z \end{pmatrix}, \tag{122b}$$

with normalization factors

$$N^+_{1,\mathrm{up}} = \sqrt{2\nu_+(\nu_+ - \mu)}, \quad N^+_{2,\mathrm{up}} = \sqrt{2\nu_+(\nu_+ + \mu)}, \tag{123a}$$

$$N^+_{1,\mathrm{down}} = \sqrt{2\nu_+(\nu_+ + \mu)}, \quad N^+_{2,\mathrm{down}} = \sqrt{2\nu_+(\nu_+ - \mu)}. \tag{123b}$$

On the intersection of their respective domains

$$\begin{array}{cccccc} \mu & |w^+_{1,\mathrm{up}}\rangle & |w^+_{1,\mathrm{down}}\rangle & |w^+_{2,\mathrm{up}}\rangle & |w^+_{2,\mathrm{down}}\rangle \\ \hline \mu<0 & \mathbb{R}^2 & \mathbb{R}^2\backslash\{0\} & \mathbb{R}^2\backslash\{0\} & \mathbb{R}^2 \\ \mu>0 & \mathbb{R}^2\backslash\{0\} & \mathbb{R}^2 & \mathbb{R}^2 & \mathbb{R}^2\backslash\{0\} \end{array}, \tag{124}$$

eigenvectors (122) are related by

$$(|w^+_{1,\mathrm{up}}\rangle, |w^+_{2,\mathrm{up}}\rangle) = (|w^+_{1,\mathrm{down}}\rangle, |w^+_{2,\mathrm{down}}\rangle)\begin{pmatrix} \zeta_1 & 0 \\ 0 & \zeta_2 \end{pmatrix}, \quad \zeta_1 = \frac{\bar\beta\bar z}{|\beta||z|} = -\zeta_2\ . \tag{125}$$

This transition relation determines the eigenspace bundle of rank two over $\mathbb{R}^2$ associatied with the eigenvalue ν_+ of K_μ.

The projection map onto the eigenspace associated with ν_+

$$P_+ = \sum_{k=1}^{2}\langle w^+_{k,\mathrm{up}}\rangle\langle w^+_{k,\mathrm{up}}| = \sum_{k=1}^{2}\langle w^+_{k,\mathrm{down}}\rangle\langle w^+_{k,\mathrm{down}}|\ .$$

defines the covariant differential operator $P_+\mathrm{d}$ with which the basis eigenvectors are operated on in order to define local connection forms. We obtain

$$\mathcal{A}^+_{\mathrm{up/down}} = \begin{pmatrix} A^+_{1,\mathrm{up/down}} & \\ & A^+_{2,\mathrm{up/down}} \end{pmatrix}, \tag{126}$$

where

$$A^{+}_{k,\mathrm{up/down}} = \langle w^{+}_{k,\mathrm{up/down}}|\,\mathrm{d}\,|w^{+}_{k,\mathrm{up/down}}\rangle, \quad k = 1, 2. \tag{127}$$

On the intersection of their respective domains, $A^{+}_{k,\mathrm{up/down}}$ are related by

$$A^{+}_{k,\mathrm{up}} - A^{+}_{k,\mathrm{down}} = \zeta_k^{-1}\mathrm{d}\zeta_k, \quad k = 1, 2. \tag{128}$$

The local curvature forms

$$\mathcal{F}^{+}_{\mathrm{up/down}} = \begin{pmatrix} F^{+}_{1,\mathrm{up/down}} & \\ & F^{+}_{2,\mathrm{up/down}} \end{pmatrix} = \begin{pmatrix} \mathrm{d}A^{+}_{1,\mathrm{up/down}} & \\ & \mathrm{d}A^{+}_{2,\mathrm{up/down}} \end{pmatrix}$$

coincide on the intersection of their respective domains and can be combined to define the global curvature form

$$\mathcal{F}^{+} = \begin{pmatrix} F^{+}_{1} & \\ & F^{+}_{2} \end{pmatrix}. \tag{129}$$

The Chern form is defined through

$$\mathrm{Det}\big(t\mathbb{1} + \frac{\mathrm{i}}{2\pi}\mathcal{F}\big) = t^2 + \frac{\mathrm{i}}{2\pi}\,t\,(F^{+}_{1} + F^{+}_{2}), \tag{130}$$

where t is a real parameter, $\mathbb{1}$ denotes the 2×2 identity matrix, and where use has been made of $F^{+}_{1} \wedge F^{+}_{2} = 0$. Thus, the first Chern form is defined to be

$$C_1 = \frac{\mathrm{i}}{2\pi}(F^{+}_{1} + F^{+}_{2}), \tag{131}$$

and the first Chern number is formally defined to be

$$c_1 = \int_{\mathbb{R}^2} C_1. \tag{132}$$

We are to observe a change in the Chern number against the control parameter μ. On account of (124), under the procedure we have frequently performed, we obtain

$$\frac{\mathrm{i}}{2\pi}\int_{\mathbb{R}^2} F^{+}_{1}|_{\mu>0} - \frac{\mathrm{i}}{2\pi}\int_{\mathbb{R}^2} F^{+}_{1}|_{\mu<0} = \frac{1}{2\pi\mathrm{i}}\int_{\Gamma}\zeta_1^{-1}d\zeta_1 = -1, \tag{133a}$$

$$\frac{\mathrm{i}}{2\pi}\int_{\mathbb{R}^2} F^{+}_{2}|_{\mu>0} - \frac{\mathrm{i}}{2\pi}\int_{\mathbb{R}^2} F^{+}_{2}|_{\mu<0} = \frac{-1}{2\pi i}\int_{\Gamma}\zeta_2^{-1}d\zeta_2 = +1, \tag{133b}$$

where Γ denotes a circle with the center at the origin of $\mathbb{R}^2$. It then follows that the change in the Chern number for the eigenspace bundle associated with the eigenvalue ν_+ of the linearized Hamiltonian K_μ at the north pole is zero;

$$c_1|_{\mu>0} - c_1|_{\mu<0} = 0. \tag{134}$$

Similar result can be obtained for the linearization at the south pole.This means that for the Hamiltonian (40) there is no modification of the Chern numbers for superbands. This result is consistent with the conservation of the number of energy levels in superbands. Nevertheless the rearrangement of superbands clearly occurs because of the modification in the decomposition of the superbands into individual irreps demostrated by correlation diagrams (see Fig 8, 10). In order to see topological modifications it is sufficient to add small perturbation breaking the Kramers degeneracy of superbands caused by $\mathcal{T}_S$ symmetry and to discuss the modifications of Chern numbers for individual components of superbands like it is done in the main text.

REFERENCES

[1] V. I. Arnold, Remarks on eigenvalues and eigenvectors of Hermitian matrices, Berry phase, adiabatic connections and quantum Hall effect, *Select. Math.*, **1** (1995), 1–19.

[2] M. F. Atiyah, V. K. Patodi and I. M. Singer, Spectral asymmetry and Riemannian geometry. I, *Math. Proc. Cambridge Phil. Soc.*, **77** (1975), 49–69.

[3] M. F. Atiyah, V. K. Patodi and I. M. Singer, Spectral asymmetry and Riemannian geometry. II, *Math. Proc. Cambridge Phil. Soc.*, **78** (1975), 405–432.

[4] M. F. Atiyah, V. K. Patodi and I. M. Singer, Spectral asymmetry and Riemannian geometry. III, *Math. Proc. Cambridge Phil. Soc.*, **79** (1976), 71–99.

[5] J. E. Avron, L. Sadun, J. Segert and B. Simon, Topological invariants in Fermi systems with time-reversal invariance, *Phys. Rev. Lett.*, **61** (1988), 1329–1332.

[6] J. E. Avron, L. Sadun, J. Segert and B. Simon, Chern numbers, quaternions, and Berry's phases in Fermi systems, *Commun. Math. Phys.*, **124** (1989), 595–627.

[7] M. Baake, A brief guide to reversing and extended symmetries of dynamical systems, in *Ergodic Theory and Dynamical Systems in Their Interactions with Arithmetics and Combinatorics* (eds. S. Ferenczi, J. Kulaga-Przymus and M. Lemanczyk), Lect. Notes Math., 2213, Springer-Verlag, Berlin, Heidelberg, 2018, 35–40.

[8] N. Berglund and B. Gentz, Deterministic slow-fast systems, in *Noise-induced Phenomena in Slow-fast Dynamical Systems*, Probability and its Applications, Springer Verlag, London, UK, 2006, 17–49.

[9] B. A. Bernevig and T. L. Hughes, *Topological Insulators and Topological Superconductors*, Princeton Univ. Press, Princeton, NJ, 2013.

[10] M. V. Berry, Quantal phase factors accompanying adiabatic changes, *Proc. Royal Soc. Lond. A*, **392** (1984), 45–57.

[11] F. Faure and B. I. Zhilinskiĭ, Topological Chern indices in molecular spectra, *Phys. Rev. Lett.*, **85** (2000), 960–963.

[12] F. Faure and B. I. Zhilinskiĭ, Topological properties of the Born–Oppenheimer approximation and implications for the exact spectrum, *Lett. Math. Phys.*, **55** (2001), 239–247.

[13] F. Faure and B. I. Zhilinskiĭ, Qualitative features of intra-molecular dynamics. What can be learned from symmetry and topology, *Acta Appl. Math.*, **70** (2002), 265–282.

[14] F. Faure and B. I. Zhilinskiĭ, Topologically coupled energy bands in molecules, *Phys. Lett. A*, **302** (2002), 985–988.

[15] B. Fedosov, *Deformation Quantization and Index Theory*, Academie Verlag, Berlin, 1996.

[16] D. Fontanari and D. A. Sadovskiĭ, Coherent states for the quantum complete rigid rotor, *J. Geom. Phys.*, **129** (2018), 70–89.

[17] J. N. Fuchs, F. Piéchon, M. O. Goerbig and G. Montambaux, Topological Berry phase and semiclassical quantization of cyclotron orbits for two dimensional electrons in coupled band models, *Eur. Phys. J. B*, **77** (2010), 351–362.

[18] F. D. M. Haldane, Model for a quantum Hall effect without Landau levels: Condensed-matter realization of the "parity anomaly", *Phys. Rev. Lett.*, **61** (1988), 2015–2018.

[19] G. Herzberg and H. C. Longuet-Higgins, Intersection of potential energy surfaces in polyatomic molecules, *Discuss. Faraday Soc.*, **35** (1963), 77–82.

[20] T. Holstein and H. Primakoff, Field dependence of the intrinsic domain magnetization of a ferromagnet, *Phys. Rev.*, **58** (1940), 1098–1113.

[21] T. Iwai and B. I. Zhilinskiĭ, Energy bands: Chern numbers and symmetry, *Ann. Phys. (NY)*, **326** (2011), 3013–3066.

[22] T. Iwai and B. I. Zhilinskiĭ, Qualitative feature of the rearrangement of molecular energy spectra from a wall-crossing perspective, *Phys. Lett. A*, **377** (2013), 2481–2486.

[23] T. Iwai and B. I. Zhilinskiĭ, Local description of band rearrangements. Comparison of semi-quantum and full quantum approach, *Acta Appl. Math.*, **137** (2015), 97–121.

[24] T. Iwai and B. I. Zhilinskiĭ, Band rearrangement through the 2D-Dirac equation: Comparing the APS and the chiral bag boundary conditions, *Indagationes Math.*, **27** (2016), 1081–1106.

[25] T. Iwai and B. I. Zhilinskiĭ, Chern number modification in crossing the boundary between different band structures: Three-band model with cubic symmetry, *Rev. Math. Phys.*, **29** (2017), 1–91.

[26] M. Kohmoto, Topological invariant and the quantization of the Hall conductance, *Ann. Phys.*, **160** (1985), 343–354.

[27] H. A. Kramers, Théorie générale de la rotation paramagnétique dans les cristaux, *Proc. Konink. Akad. Wetensch.*, **33** (1930), 959–972, URL http://www.dwc.knaw.nl/DL/publications/PU00015981.pdf.
[28] J. S. W. Lamb, Reversing symmetries in dynamical systems, *J. Phys. A*, **25** (1992), 925–937.
[29] J. S. Lamb and J. A. Roberts, Time-reversal symmetry in dynamical systems: A survey, *Physica D*, **112** (1998), 1–39.
[30] Y. Lee Loh and M. Kim, Visualizing spin states using the spin coherent state representation, *Am. J. Phys.*, **83** (2015), 30–35.
[31] C. A. Mead, Molecular Kramers degeneracy and non-Abelian adiabatic phase factors, *Phys. Rev. Lett.*, **59** (1987), 161–164.
[32] C. A. Mead and D. G. Truhlar, On the determination of Born–Oppenheimer nuclear motion wave functions including complications due to conical intersections and identical nuclei, *J. Chem. Phys.*, **70** (1979), 2284–2296.
[33] M. Moshinsky and A. Szczepaniak, The Dirac oscillator, *J. Phys. A: Math. Gen.*, **22** (1989), L817–L819.
[34] A. I. Neishtadt and A. A. Vasiliev, Destruction of adiabatic invariance at resonances in slow-fast Hamiltonian systems, *Nucl. Instr. Meth. A*, **561** (2006), 158–165.
[35] A. I. Neishtadt, Averaging method and adiabatic invariants, in *Hamiltonian Dynamical Systems and Applications* (ed. W. Craig), NATO science for peace and security series B: Physics and Biophysics, Springer Science, Netherlands, 2008, 53–66.
[36] V. B. Pavlov-Verevkin, D. A. Sadovskiĭ and B. I. Zhilinskiĭ, On the dynamical meaning of the diabolic points, *Europhysics Letters*, **6** (1988), 573–8.
[37] D. A. Sadovskiĭ and B. I. Zhilinskiĭ, Monodromy, diabolic points, and angular momentum coupling, *Phys. Lett. A*, **256** (1999), 235–44.
[38] B. Simon, Holonomy, the quantum adiabatic theorem, and Berry's phase, *Phys. Rev. Lett.*, **51** (1983), 2167–2170.
[39] D. J. Thouless, *Topological Quantum Numbers in Nonrelativistic Physics*, World Scientific, Singapore, 1998.
[40] D. J. Thouless, M. Kohmoto, M. P. Nightingale and M. den Nijs, Quantized Hall conductance in a two-dimensional periodic potential, *Phys. Rev. Lett.*, **49** (1982), 405–408.
[41] J. von Neumann and E. P. Wigner, Über merkwürdige diskrete Eigenwerte. Über das Verhalten von Eigenwerten bei adiabatischen Prozessen, *Physicalische Z.*, **30** (1929), 467–470.
[42] E. P. Wigner, Über die Operation der Zeitumkehr in der Quantenmechanik, *Nachr. Akad. Ges. Wiss. Göttingen*, **31** (1932), 546–559.
[43] F. Wilczek and A. Shapere, *Geometric Phases in Physics*, Advanced Series in Mathematical Physics, 5, World Scientific, 1989.
[44] R. N. Zare, *Angular Momentum: Understanding Spatial Aspects in Chemistry and Physics*, Wiley, New York, 1988.
[45] W.-M. Zhang, D. H. Feng and R. Gilmore, Coherent states: Theory and some applications, *Rev. Mod. Phys.*, **62** (1990), 867–927.

Received September 2019; revised February 2020.

E-mail address: iwai.toshihiro.63u@st.kyoto-u.ac.jp
E-mail address: sadovski@univ-littoral.fr
E-mail address: zhilin@univ-littoral.fr